Marine Geology 429 (2020) 106312

Contents lists available at ScienceDirect

Marine Geology

journal homepage: www.elsevier.com/locate/margo

Controls on the spatio-temporal distribution of microbialite crusts on the Great Barrier Reef over the past 30,000 years

Zs. Szilagyi[a,b,*], Jody M. Webster[a], Madhavi A. Patterson[a], Kinga Hips[c], Robert Riding[d], Matthew Foley[e], Marc Humblet[f], Yusuke Yokoyama[g], Liyuan Liang[d], Eberhard Gischler[h], Lucien Montaggioni[i], Douglas Gherardi[j], Juan C. Braga[k]

[a] Geocoastal Research Group, School of Geosciences, The University of Sydney, Australia
[b] Department of Physical and Applied Geology, Institute of Geography and Earth Sciences, Eötvös Loránd University, Hungary
[c] MTA-ELTE Geology, Geophysics and Space Science Research Group, Eötvös Loránd University, Hungary
[d] Department of Earth and Planetary Sciences, University of Tennessee, 1621 Cumberland Avenue, Knoxville, TN 37996-1526, USA
[e] Australian Centre for Microscopy & Microanalysis, The University of Sydney, Australia
[f] Department of Earth and Planetary Sciences, Nagoya University, Japan
[g] Atmosphere and Ocean Research Institute, Department of Earth and Planetary Sciences, University of Tokyo, Japan
[h] Department of Geosciences, Goethe University, Frankfurt, Germany
[i] CEREGE, Aix-Marseille University, CNRS, IRD, Collège de France, St Charles, 13331, Marseilles, France
[j] National Institute for Space Research, Sao Jose dos Campos, Brazil
[k] Department of Stratigraphy and Paleontology, University of Granada, Spain

ARTICLE INFO

Keywords:
Reefal microbialite
Quaternary reef systems
3D visualization
Paleo-proxy
Ocean acidification

ABSTRACT

Calcification of microbial mats adds significant amounts of calcium carbonate to primary coral reef structures that stabilizes and binds reef frameworks. Previous studies have shown that the distribution and thicknesses of late Quaternary microbial crusts have responded to changes in environmental parameters such as seawater pH, carbonate saturation state, and sediment and nutrient fluxes. However, these studies are few and limited in their spatio-temporal coverage. In this study, we used 3D and 2D examination techniques to investigate the spatio-temporal distribution of microbial crusts and their responses to environmental changes in Integrated Ocean Drilling Program (IODP) Expedition 325 (Great Barrier Reef Environmental Changes) fossil reef cores that span 30 to 10 ka at two locations on the GBR reef margin. Our GBR microbialite record was then combined with a meta-analysis of 17 other reef records to assess global scale changes in microbialite development (i.e., presence/absence, thickness) over the same period. The 3D results were compared with 2D surface area measurements to assess the accuracy of 2D methodology. The 2D technique represents an efficient and accurate proxy for the 3D volume of reef framework components within the bounds of uncertainty (average: 9.45 ± 4.5%). We found that deep water reef frameworks were most suitable for abundant microbial crust development. Consistent with a previous Exp. 325 study (Braga et al., 2019), we also found that crust ages were broadly coeval with coralgal communities in both shallow water and fore-reef settings. However, in some shallow water settings they also occur as the last reef framework binding stage, hundreds of years after the demise of coralgal communities. Lastly, comparisons of crust thickness with changes in environmental conditions between 30 and 10 ka, show a temporal correlation with variations in partial pressure of CO_2 (pCO_2), calcite saturation state ($\Omega_{calcite}$), and pH of seawater, particularly during the past ~15 kyr, indicating that these environmental factors likely played a major role in microbialite crust development in the GBR. This supports the view that microbialite crust development can be used as an indicator of ocean acidification.

1. Introduction

Coral reef ecosystems are highly sensitive to rapid environmental changes (Pandolfi et al., 2003; Hughes et al., 2007; Hughes et al., 2010) such as fluctuation in water depth, light, hydrodynamic energy, temperature, and water chemistry and quality (Webster et al., 2009; Abbey et al., 2011; Woodroffe and Webster, 2014).

Reef frameworks built by corals and coralline algae can be highly

* Corresponding author at: Geocoastal Research Group, School of Geosciences, The University of Sydney, Australia.
E-mail address: zsan.szilagyi@hotmail.com (Z. Szilagyi).

https://doi.org/10.1016/j.margeo.2020.106312
Received 7 April 2020; Received in revised form 27 July 2020; Accepted 28 July 2020
Available online 05 August 2020

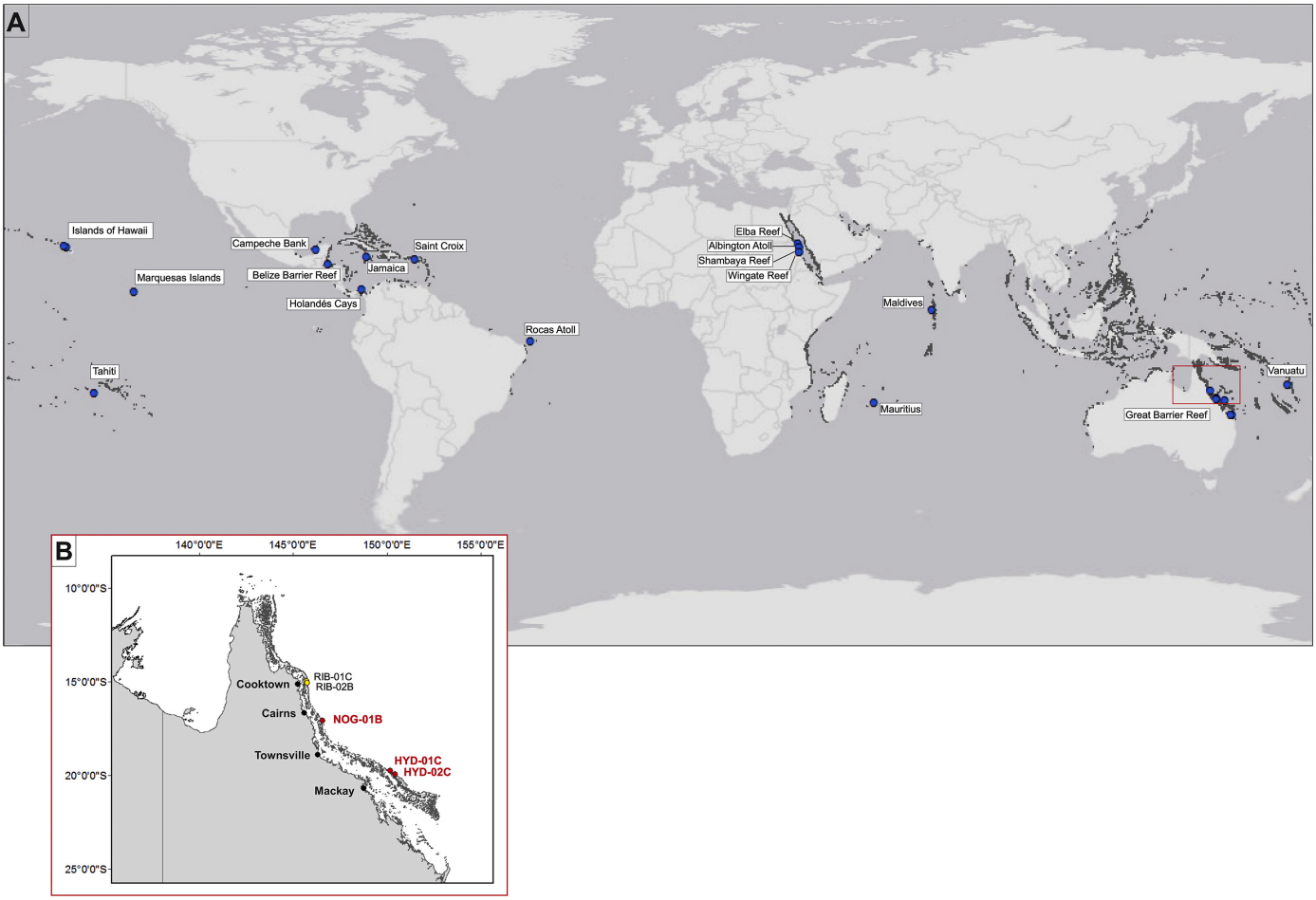

Fig. 1. Location map of microbial crusts in reef systems in the last 30 kyr. (A) Spatial distribution of microbial crusts from around the world over the last 30 kyr (Source map: Esri, DigitalGlobe, GeoEye, Earthstar Geographics, CNES/Airbus DS, USDA, USGS, AeroGRID, IGN, and the GIS User Community). (B) Integrated Ocean Drilling Program Expedition 325, Great Barrier Reef, Australia, transects location. RIB-01C and 02B: Ribbon Reef (Offshore Cooktown); NOG—01B: Noggin Pass (Offshore Cairns); HYD-01C and 02C: Hydrographer's Passage (Offshore Mackay).

cavernous, providing extensive habitats for cryptic organisms (Ginsburg, 1983). In addition to skeletal encrusters such as bryozoans, serpulids, foraminifers and sponges, recent reef crypts can host biofilm crusts (Montaggioni and Camoin, 1993; Riding, 2011), as well as sediments (Insalaco, 1998).

Microbial crusts in late Pleistocene and Holocene reefs were initially commonly regarded as fine-grained cements (Macintyre, 1977). They are typically composed of magnesium calcite, and appear to preferentially develop in cavities on high-energy reef margins (Macintyre, 1977). Analyses indicate abundant biomarkers with intermediate-to-high specificity for sulfate-reducing bacteria (Heindel et al., 2010, 2012), confirming earlier suggestions (Land and Goreau, 1970; Pigott and Land, 1986). Well-known examples of fossil microbialites include the late Miocene of Spain (Riding, 1991) and the late Quaternary of Tahiti (Montaggioni and Camoin, 1993; Camoin and Montaggioni, 1994; Camoin et al., 1999; Seard et al., 2011; Riding et al., 2014) and the GBR (Webb and Jell, 1997; Webb et al., 1998; Webb and Jell, 2006; Jell and Webb, 2012; Braga et al., 2019), in which microbial crusts can be dominant components, both structurally and in abundance, locally representing up to 80% of the total reef volume. These reefal microbial crusts appear to be largely precipitated and have distinctive clotted-peloidal fabrics in addition totrapped and bounded detritus (Riding, 2011).

These microbial crusts stabilize the framework and build a robust substrate that can be used by reef builders to colonize and grow (Riding, 1991; Beltrán et al., 2016). Furthermore, Webb and Kamber (2000) suggested that they are a reliable seawater REE paleoproxy, and can provide information about their depositional environment, including oceanic oxygenation and the input of terrestrial detritus.

Microbial crusts are likely not as sensitive as corals and coralline algae to light and depth changes but they can show substantial variations in their thickness and distribution within reef frameworks in response to environmental changes (Camoin and Montaggioni, 1994, Riding et al., 2014). Late Pleistocene reef systems are reported to have more abundant microbial crusts, while they are less abundant in shallow Holocene coral reef frameworks (Heindel et al., 2010; Jell and Webb, 2012). According to Cabioch et al. (2006) their distribution in Vanuatu reefs between 24 and 6 ka was due to higher nutrient supply associated with periods of rapid sea-level rise. Other studies in the Pacific, Atlantic and Indian Oceans (Tahiti, Belize and Maldives) have linked increased abundance of microbial crusts to enhanced nutrient fertilization (Camoin and Montaggioni, 1994; Camoin et al., 1999; Camoin et al., 2006; Heindel et al., 2009; Heindel et al., 2010; Heindel et al., 2012). However, according to Riding et al. (2014) the crust thickness depends more on seawater pH, and carbonate saturation state ($\Omega_{calcite}$), together with the space available for development within the framework. Riding et al. (2014) suggested that microbial crust development could be a sensitive indicator of early changes in ocean acidification and therefore potentially a paleo pH proxy. To assess the validity of this model, additional data, over longer time scales and over numerous interglacial and glacial cycles are required.

The objective of this study is to better understand the factors that

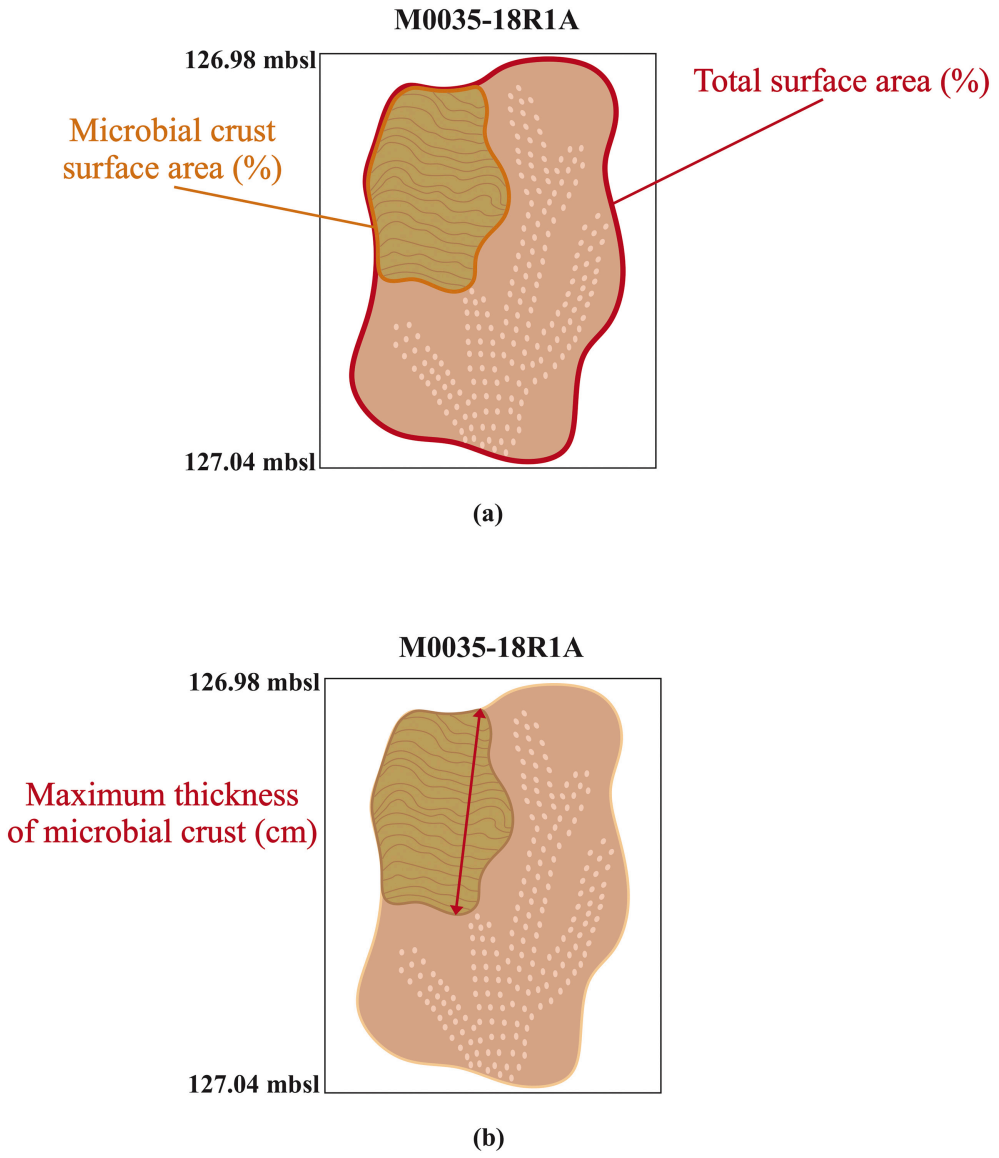

Fig. 2. Illustration showing the 2D measurement approach using an idealized section. (a) Surface area calculation of the microbial crusts. (b) Thickness calculation of microbial crusts.

controlled microbial crust formation during the last glacial maximum (LGM) and deglacial reef development in the GBR based on samples recovered by IODP Expedition 325. We test the hypothesis that crust thickness and volume reflect ocean pH and $\Omega_{calcite}$ (Riding et al., 2014; Braga et al., 2019) and further assess the role of microbialites in reef framework development and preservation. Expedition 325 cores represent a high resolution record of reef development associated with microbial crusts for the interval between 30 and 10 ka (Webster et al., 2018; Yokoyama et al., 2018; Braga et al., 2019). 3D X-ray computed tomography (CT) scan image analysis is used to assess the 3D heterogeneity (occurrence, geometry, volume) of the microbial crusts. These results are then compared to 2D surface area measurements from the entire core data set to obtain an accurate estimate of microbialite surface area (abundance). Our Expedition 325 microbial crust thickness and volume estimates, combined with a robust chronologic framework provided by 32 new and 27 existing radiocarbon dates, allow us to explore crust development relative to other reef framework builders, as well as to environmental changes between 30 and 10 ka. Finally, we combine our Expedition 325 results, with a comprehensive meta-analysis of published literature to assess major controls on microbial crust development over the past 30 kyr.

2. Geological setting and previous work

In 2010, IODP 325 recovered fossil coral reef cores from the shelf edge of the GBR. Thirty-four holes were drilled at 17 sites (M0030-M0058A) along four transects at three locations (Hydrographer's Passage, Noggin Pass and Ribbon Reef) between 42 and 157 m below sea level (mbsl) (Fig. 1). The main scientific objectives of Exp. 325 were to reconstruct the nature of sea level and sea surface temperatures during the LGM to deglaciation, and to assess the impact of these and associated environmental changes on the evolution of the GBR over this period. The ages of the reef deposits recovered range from 9 ka to > 30 ka (Webster et al., 2011; Yokoyama et al., 2011; Webster et al., 2018; Yokoyama et al., 2018). Five main reef sequences were defined: Reef 1 (≥ MIS 3), Reef 2 (27–22 ka), Reef 3a (21–17 ka), Reef 3b (17–13 ka), Reef 4 (13–10 ka), and Reef 5 (10–1 ka) (Webster et al., 2018). Webster et al. (2018) and Humblet et al. (2019) reported six different coral assemblages in the Exp. 325 cores: (1) A (mlsoAcro) (massive/ robust branching *Isopora* and corymbose *Acropora* gr. *humilis)*, (2) B (bSeriAcro) (branching *Seriatopora, Acropora* sp.), (3) C (meMer) (massive/ encrusting merulinids, (4) D (mP) (massive *Porites*), (5) E (esmPM) (encrusting/ submassive *Porites* and *Montipora*), and (6)

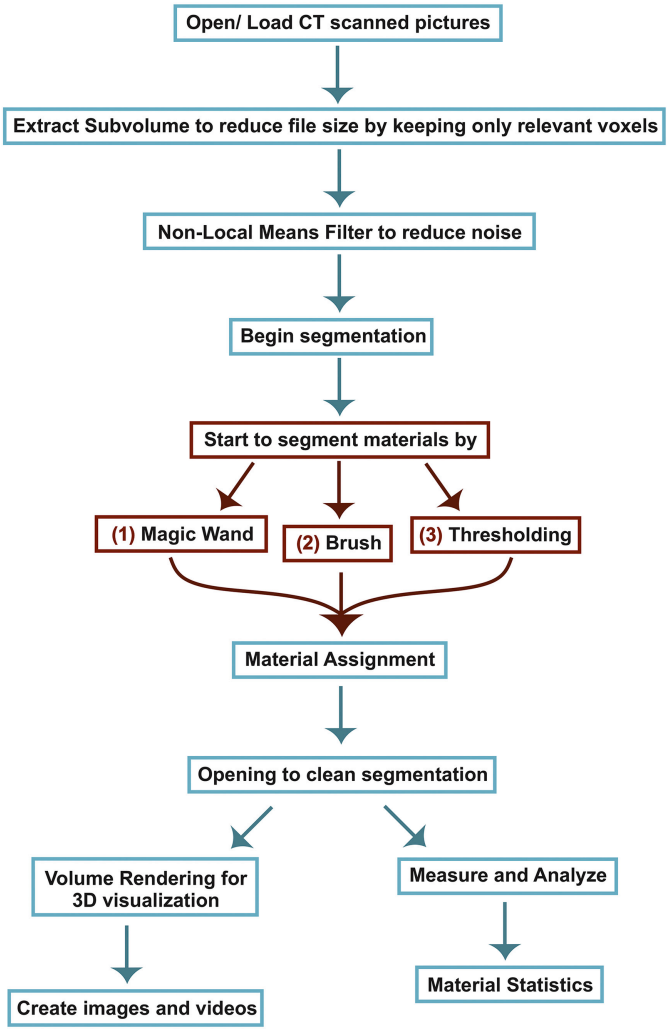

Fig. 3. Workflow for the 3D visual analysis. Blue brackets indicate commands where the software is running automatically while red brackets indicate those requiring an operator decision. Irrelevant voxels (predominantly air surrounding the samples) were excluded from analysis through a sub-volume selection, after which filtering was performed to reduce noise. Segmentation of the data to the individual materials was performed using the following built-in tools: (1) Magic Wand, (2) manual Brush, and/or (3) Thresholding. Binary opening was applied to clean the segmentation to avoid any misidentification due to partial voxel averaging. Measurement of the segmented materials was performed using the Material Statistics module (i.e. to calculate volume), while the segmented and processed data was Volume Rendered to create representative visual images and videos. (For interpretation of the references to colour in this figure legend, the reader is referred to the web version of this article.)

F (eAg) (encrusting/ foliaceous agariciids). Braga et al. (2019) described both reefal and fore-reef microbial crusts and concluded that the microbialites were likely formed by sulfate-reducing bacteria in anoxic microenvironments during the LGM and early deglaciation. These crusts developed in the photic zone, but not necessarily all were in illuminated environments. Two main types of occurrence were distinguished: (i) reefal microbial crusts in reef-framework cavities, and (ii) fore-reef microbialites formed on the sea floor, and in cavities generated by larger bioclasts and encrusting corals (Braga et al., 2019).

In this study, we focus on microbialites recovered from two transects at Hydrographer's Passage (HYD-01C and HYD-02A) and Noggin Pass (NOG−01B) (see Webster et al., 2018 for detailed site information) (Fig. 1B).

3. Methodology

3.1. 2D surface area and thickness calculation of microbial crusts

High resolution images were used to collect two datasets 1) the 2D surface area, and 2) the maximum thickness of microbial crusts in cores from HYD-01C and NOG-01B transects (Braga et al., 2019).

Building on Braga et al. (2019) surface area dataset, a more detailed quantification of 1) total surface area and 2) surface area of microbial crust for each sample within a recovered core was conducted using Adobe Illustrator CS6 add-on Patharea Filter plug-in (Fig. 2a). Percentage of microbialite from the total recovered surface area were then calculated (microbialite surface area/total surface area = percentage microbialite surface area) and analyzed in comparison to 3D volume calculations described in Section 3.3.

The maximum thickness of each microbial crust was measured perpendicular to crust lamination or growth surface directions using Adobe Illustrator CS6 (Fig. 2b).

The Exp. 325 data sets were also aggregated and statistical analyses were carried out to best quantitatively assess trends in the microbialite thickness and surface area data. Regression analysis was applied to the surface area and maximum thickness data. This approach was also applied to the global thickness datasets while separating the data from Tahiti, the GBR, and the other Holocene locations. Microbialite thickness values from the GBR were also compared with calcite saturation state (using data in Fig. 6 of Riding et al., 2014) and reef accretion rates (using data in Table S2 of Webster et al., 2018) at that time to assess their correlation.

3.2. 3D volumetric calculation of microbial crusts

Representative Exp. 325 cores were computed tomography (CT) scanned and analyzed to assess the 3D heterogeneity (occurrence, geometry, and volume) of the microbial crusts in the reef frameworks. Detailed 3D visualization and analysis of microbial crusts from four representative cores was carried out: (1) M0035A-17R1A (41 cm), (2) M0035A-18R1A (45 cm), (3) M0035A-19R1A (68 cm) from Hydrographer's Passage site, and (4) M0054B-6R1A (140 cm) from Noggin Pass site. The representative core sections were selected for the following criteria: (1) well developed microbial crusts, (2) distinct geographic locations (Hydrographer's Passage, Noggin Pass), (3) distinct reef environments (shallow vs. deep), (3) similar age ranges (~20.8 – ~20 ka) but different reef sequences (Reef 2, Reef 3a), and (4) a range of different coral assemblages and framework types.

The cores were scanned using an X-ray CT Scanner (spatial resolution: 0.31 mm/pixel; scanning time: 0.6, 1, 2, 4 s; field of view: 160–180 mmp) at the IODP Kochi Core Center, Japan. CT is a non-destructive technique to produce images of the interior characters of solid objects. Using the variation of X-ray attenuation within the objects, images can be created to reconstruct their 3D geometries and properties (Ketcham and Carlson, 2001; Carlson, 2006).

3D visual analysis of cores was made using AVIZO 9.4 software on CT-Scan data at the Australian Centre for Microscopy and Microanalysis, The University of Sydney.

AVIZO is a 3D visualization and analysis software for scientific and industry X-ray CT data. It allowed us to separate and label microbial crusts, corals and coralline algae, rubble and unconsolidated sediment using the built-in segmentation tools (i.e., 'Magic Wand' region selector, 'manual brush') and interpolation between slices where appropriate (Fig. 3). Voxels were assigned to the different materials (air, microbial crust, coral and coralline algae, rubble and unconsolidated sediment) based on observed grayscale intensities which represent different attenuation values. The term rubble was used for broken core material composed of a mixture of coralgal and microbialite material. The assignments of the intensity levels to the separate materials were based on operator comparison of structural features observed in the CT data as

compared to optical high-resolution images taken previously. After labelling the distinguished components, volumetric calculation and imaging of the materials were undertaken. The scan voxel resolutions are 0.27 × 0.27 × 0.625 mm and 0.18 × 0.18 × 0.625 mm. A similar approach was carried out by Seard et al. (2011) on Tahiti cores from IODP Expedition 310.

The 3D scanned results were converted to percentages of the total recovered sample volume values and directly compared to the 2D surface area percentage of microbialite (described Section 3.1). Unlike the 2D method, the 3D method accounted for the 3D heterogeneity of microbialite development in reef frameworks (Seard et al., 2011). This allowed us to quantitatively assess the accuracy of our 2D surface area calculations - which were calculated for the entire Exp. 325 core data set (Braga et al., 2019) - compared with the 3D CT scan approach that calculated the volume only 4 representative core sections. These analyses and their comparison allowed us to describe the stratigraphic distribution of microbial crust in the two locations, and to compare the relative abundance of different reef components.

3.3. Microbial crust age model

Ages were assigned to the microbialite data set (surface area and thickness) based on the vertical accretion model developed by Webster et al. (2018) that involves defining linear growth segments between distinct inflection points in the vertical reef accretion history. The segments are based on > 500 calibrated ^{14}C AMS coral and coralline algae and in-situ U/Th coral ages (Webster et al., 2011; Gischler et al., 2013; Felis et al., 2014; Yokoyama et al., 2018). In the current study, microbialite age estimates were obtained by using the visual fit equation of segments and the average depth of the measured microbial crusts.

3.4. Comparison of radiocarbon ages of corals and microbial crust and coralline algae and microbial crusts

Corals, coralline algae crusts (27 samples) and microbial crusts (32 samples) from existing and new samples were radiocarbon dated to compare the ages of corals/ coralline algae and the microbialite directly encrusting them in 19 cases. Selected components were dated by Single Stage Accelerator Mass Spectrometry at the Atmosphere and Ocean Research Institute (AORI), the University of Tokyo, Japan and at the Australian National University (ANU). During processing, samples were converted into graphite at AORI and generally 1 mg of them was measured (Yokoyama et al., 2018).

To directly compare the ages of microbial crusts, corals and coralline algae, uncalibrated ^{14}C ages were used following Seard et al. (2011). Using calibrated and corrected ages may introduce an additional error (e.g., from reservoir correction, from variation in the calibration curve, from standard error for predicted values) which increases the calibrated age range (Stuiver and Braziunas, 1993; Reimer et al., 2013; Cook et al., 2015). Accordingly, age data from the same sample and sampling location and context were selected and compared (Fig. 4A); where there was more than one measurement for the same material the average of their ages was used. For the age offset (Δ) calculation between corals and microbial crusts and coralline algae and microbial crusts, the midpoint of 1σ value of raw ^{14}C ages was used. To calculate the errors of the offsets we used the following equation:

$$e_d = \frac{\sqrt{(e_1^2 + e_2^2 + \ldots)}}{\sqrt{n}}$$

where e_d: age difference error, e_1: age 1 error, e_2: age 2 error and n: sample number. We calculated the confidence interval of the population with confidence level of 95% by using the equation $[u_\alpha\sigma + \mu; -u_\alpha\sigma + \mu]$ with $u_{0.05} = 2$ where μ: mean of the population and σ: standard deviation of the population (after Seard et al., 2011).

4. Results

4.1. Comparison of volumetric and surface area calculations

The results of 2D and 3D measurement techniques show some differences in the four selected core sections (Fig. 5, Table 1). In the 3D volume calculation, mainly in situ corals and coralline algae and rubble were identified in addition to microbialites in section M0035A-17R1A (Fig. 6), M0035A-18R1A (Fig. 7) and M0054B-6R1A (Fig. 9). Only M0035A-19R1A (Fig. 8) contained a fifth component, i.e., unconsolidated sediment (8.58%) (Fig. 5, Table 1, and see supplementary for videos). The 2D measurement technique estimated only the percentage of the total core section surface area composed of microbial crusts. Coral and coralline algae content (percentage of the total volume of recovered core material) is highest in section M0035A-18R1A (38.86%) and lowest in section M0035A-19R1A (15.2%). The highest rubble content was measured in section M0035A-17R1A (27.81%) and the lowest occurs in section M0054B-6R1A (0.63%). Based on the 3D measurements, section M0054B-6R1A contains the largest volume of microbialite (72.66%) and section M0035A-17R1A shows the lowest value (43.18%). The 2D technique estimated the largest surface area occupied by microbialites in section M0035A-19R1A (67.02%) and the smallest in section M0035A-18R1A (49%). In both sections M0035A-17R1A and M0035A-19R1A, the 2D technique shows microbialite content values higher by 8.61% and 3.36%, respectively, compared with the 3D technique. However, in sections M0035A-18R1A and M0054B-6R1A the 3D volumetric values are higher by 11.36% and 14.2%, respectively, compared with the 2D surface measurement method. In summary, the difference between the two techniques is relatively small; the discrepancy between the percentages of volume and surface area occupied by microbial crusts is 3–15%, and is on average 9.45%, with a standard error of 4.5%.

This discrepancy most likely derives from using different classification methods for microbial crusts in the 2D and 3D analyses and from the difficulty in identifying microbialite in rubble based on the 3D method. The mesoscale fabric classification of Braga et al. (2019) was followed during 3D visual analysis: (1) laminated, (2) structureless, (3) digitated, (4) intraskeletal and boring-fill, and (5) microbialite coated debris (MCD). During 2D surface area analysis, the classification of Montaggioni and Camoin (1993), Camoin and Montaggioni (1994), Camoin et al. (1999), Camoin et al. (2006), Cabioch et al. (2006), and Seard et al. (2011) was used in addition to Braga et al. (2019). In these earlier works, MCD is not distinguished. MCD is described as a breccia of large bioclasts coated by microbial carbonate, where clasts can be several centimeters in size and microbialites are preserved in growth position (Braga et al., 2019). During 2D and 3D analysis the sizes of the MCD parts of the cores may have been identified differently, resulting in variations between the two techniques. Another reason for differences between 2D and 3D measurements may be due to the difficulty in distinguishing rubble pieces and microbial crusts in grayscale X-ray images used for the 3D analysis; some may have been labelled as 'rubble' despite the possibility that they may contain microbialite. In contrast, high-resolution pictures enable rubble and microbialite to be distinguished with a higher level of confidence.

Despite these differences, the results suggest that 2D surface area measurement is a robust method that can closely approximate the volume of microbialite making up the reef framework. As the two measurements were in general agreement, the surface area values, which covered the entire dataset, were used for further analysis in combination with the separate maximum thickness dataset to investigate the stratigraphic and temporal variations in microbialite abundance

4.2. Stratigraphic distribution of microbial crusts in northern Hydrographer's Passage and Noggin Pass transects

In both transects, holes were drilled in four different locations of the

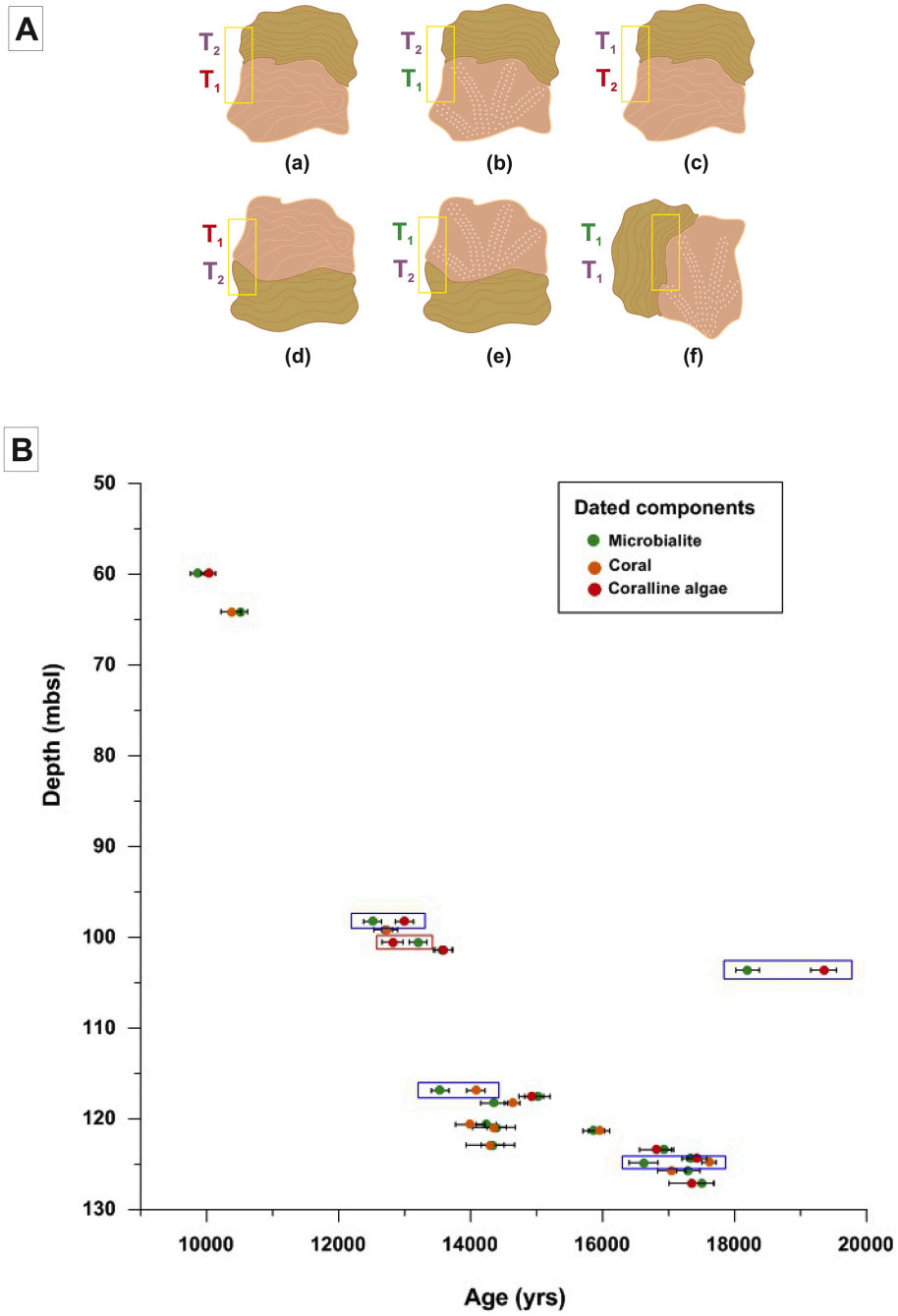

Fig. 4. Timing of microbial crust development. (A) Sampling locations (yellow rectangle) for radiocarbon dating showing the different topological positions of the dated microbial crusts, corals and coralline algae, and their chronostratigraphic relationships. (a) Coralline algae (bottom) overlain by younger microbial crusts (top). (b) Coral (bottom) overlain by younger microbial crusts (top). (c) Coralline algae (bottom) overlain by older microbial crusts. (d) Microbial crusts overlain by older coralline algae, (e) or coral. (f) Microbial crusts adjacent to a coral with the same age. (B) Uncalibrated ^{14}C age microbialite (green), coral (orange), and coralline algae (red) with 2σ value versus depth from IODP Exp. 325 cores (ages of corals and coralline algae are from Yokoyama et al., 2018). Blue rectangles represents the values where microbialite is younger than its substrate. The red rectangle show the ages where microbialite is older, despite it is topologically above its substrate. (For interpretation of the references to colour in this figure legend, the reader is referred to the web version of this article.)

shelf (Hinestrosa et al., 2016; Webster et al., 2011, 2018): inner or outer barrier, inner terraces, mid terraces and outer terraces (Fig. 10). Microbial crusts occurred in all locations but their distribution and surface area values vary considerably with depth. Braga et al. (2019) compared the stratigraphic distribution of microbialites against lithology and paleoenvironment, in this study their spatio-temporal distribution is compared with that of coral assemblages reported in Webster et al. (2018) and Humblet et al. (2019).

The outer terrace of Hydrographer's Passage (HYD−01C) (hole 39A) shows microbialite surface area increase between ~130 mbsl and ~123 mbsl and decrease between ~123 mbsl and ~111 mbsl (Fig. 10A). Microbial crusts occur in microbialite boundstone, coralgal boundstone and rudstone in association with coral assemblage A, B, D and E (Webster et al., 2018; Humblet et al., 2019). The mid-terrace hole 35A shows a relatively high microbialite content between depths of ~131 mbsl and ~111 mbsl, while in hole 36A, there is a peak at ~114 mbsl. Microbial crusts are observed in coralgal-microbial boundstone and rudstone, mainly with coral assemblages A, B, C, E, and F (Webster et al., 2018; Humblet et al., 2019). Holes 31A, 32A, and 33A on the inner terraces display differences despite their geographic proximity. Hole 33A shows relatively high crust surface area compared to holes 31A and 32A. Microbial crusts occur mostly in coralgal-microbialite boundstone, and to a lesser extent in rudstone, coralgal boundstone, and unconsolidated sediments. Microbial crusts are associated with coral assemblage A, B, C, D and E (Webster et al., 2018; Humblet et al., 2019). In hole 34A on the outer barrier, the abundance of microbial crusts peaks at ~67 mbls, ~64 mbsl and ~58 mbsl. In this hole microbialites occur in coralgal-microbialite boundstone with coral assemblage A (Webster et al., 2018; Humblet et al., 2019).

Holes from the more northern Noggin Pass (NOG−01B) transect display patterns of microbialite thickness and distribution that differ from the HYD-01C transect (Fig. 10B). In mid and outer terraces, higher

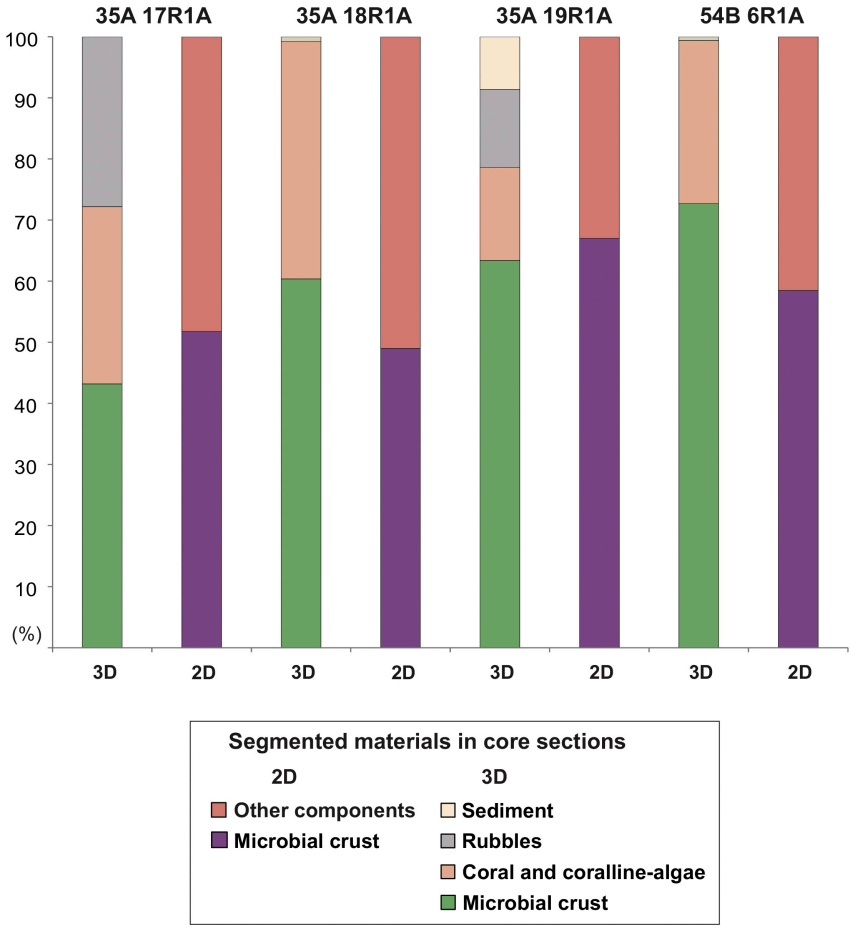

Fig. 5. Comparison of the percentages of microbial crusts calculated using the 2D and 3D technique in core sections M0035A-17R1A, −18R1A and -19R1A and M0054B-6R1A. For the 2D surface area measurements, the percentage of microbial crusts is displayed in purple and the percentage of the remaining components is indicated in dark pink. For the 3D volumetric measurements the percentage of microbial crusts is in green, the percentage of corals and coralline algae in light orange, the percentage of rubbles in grey, and the percentage of unconsolidated sediments in light pink. (For interpretation of the references to colour in this figure legend, the reader is referred to the web version of this article.)

Table 1
Summary of results of 3D visual analysis and 2D surface area measurements in the selected core sections.

Core ID	M0035A-17R1A	M0035A-18R1A	M0035A-19R1A	M0054B-6R1A
Location	HYD-01C	HYD-01C	HYD-01C	NOG-01B
Recovered core length (cm)	41	45	68	140
Depth (mbsl)	125.48–125.89	126.98–127.43	128.48–129.16	123.73–125.13
Age (ka)	20.03–20.24	20.17–20.42	n.a.	20.31–20.75
Lithology	Coralgal-microbialite boundstone	Coralgal-microbialite boundstone	Microbialite boundstone	Microbialite boundstone
CT scan resolution	0.27 × 0.27 × 0.625	0.27 × 0.27 × 0.625	0.18 × 0.18 × 0.625	0.18 × 0.18 × 0.625
2D surface area of microbialite (%)	51.79	49.00	67.02	58.47
2D surface area of other components (%)	48.21	51.00	32.98	41.53
3D volume of microbialite (%)	43.18	60.36	63.39	72.66
3D volume of coral and coralline algae (%)	29.02	38.86	15.20	26.70
3D volume of rubble (%)	27.81	0.77	12.84	0.63
3D volume of unconsolidated sediment (%)	0	0	8.58	0

microbial crust surface area is recorded in the deeper core sections. In hole 53A a decreasing upcore trend is observed, while hole 54B displays continuously high values between ~129 and ~123 mbsl. Hole 54A is a short core but also shows increasing crust surface area with depth. In these holes, microbial crusts are associated with various facies, i.e., microbialite boundstone, coralgal-microbialite boundstone, and coralgal boundstone, and occur with diverse coral assemblages, such as A, B, C, and E (Webster et al., 2018; Humblet et al., 2019). Hole 55A on the inner terraces shows upcore increase in surface area values with a peak around ~101 mbsl followed by decreasing values. In hole 56A microbial crusts are relatively poorly developed; they occur in coralgal boundstone and coralgal-microbialite boundstone, and are associated with coral assemblages A, B, C, D and E (Webster et al., 2018; Humblet et al., 2019). Hole 57A was drilled in the inner barrier and is characterized by a relatively high microbial crust surface area at a depth of ~61–63 mbsl in coralgal-microbialite boundstone containing coral assemblage A (Webster et al., 2018; Humblet et al., 2019).

The trend in the microbialite surface area data is consistent with the trend in thickness values through time (Supplementary Fig. 1D and E). There is no significant pattern at HYD, whereas surface area values are more consistent with thickness values at NOG. According to regression analysis (Fig. 11), microbialite surface area shows a generally decreasing trend through time between ~30 and ~10 ka at HYD (Fig. 11B). In contrast, there is an increasing trend between ~30 and ~19 ka and then a decreasing trend from ~19 to ~10 ka at NOG (Fig. 11C). The lack of clear temporal trend at HYD could relate to the lower recovery and less continuous reef record at HYD compared to NOG (Webster et al., 2018).

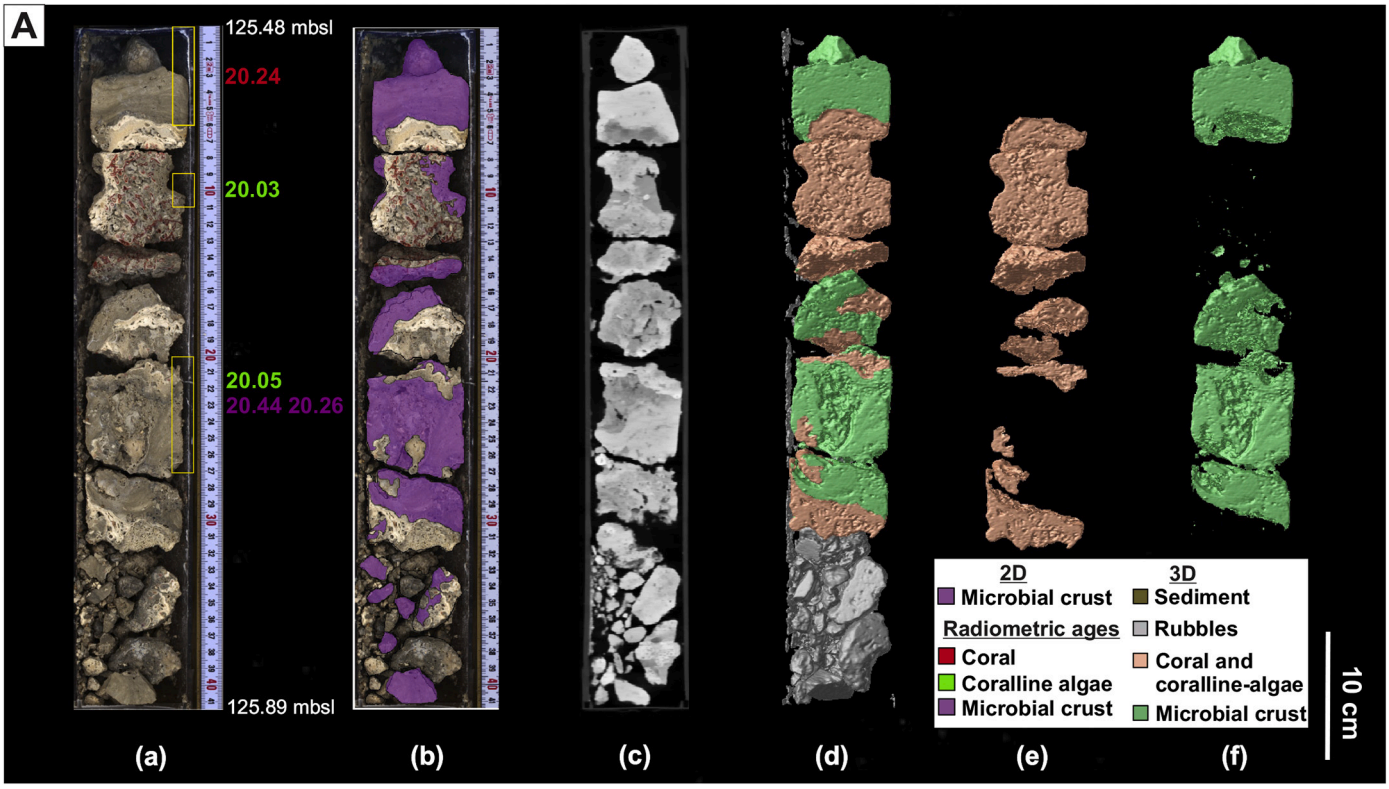

Fig. 6. Results of 3D and 2D analyses of core section M0035A-17R1A (125.48–125.89 mbsl). (a) High-resolution core image with locations of dated samples (yellow rectangle) and their radiometric ages (purple: microbial crusts, green: coral, red: coralline algae). (b) 2D analyses of the high-resolution picture where the surface area occupied by microbial crusts is indicated in purple. (c) CT-scan of the core section. (d) 3D image displaying corals and coralline algae in pink, microbial crusts in green and rubble in grey. (e) 3D image of corals and coralline algae. (f) 3D image of microbial crusts. (For interpretation of the references to colour in this figure legend, the reader is referred to the web version of this article.)

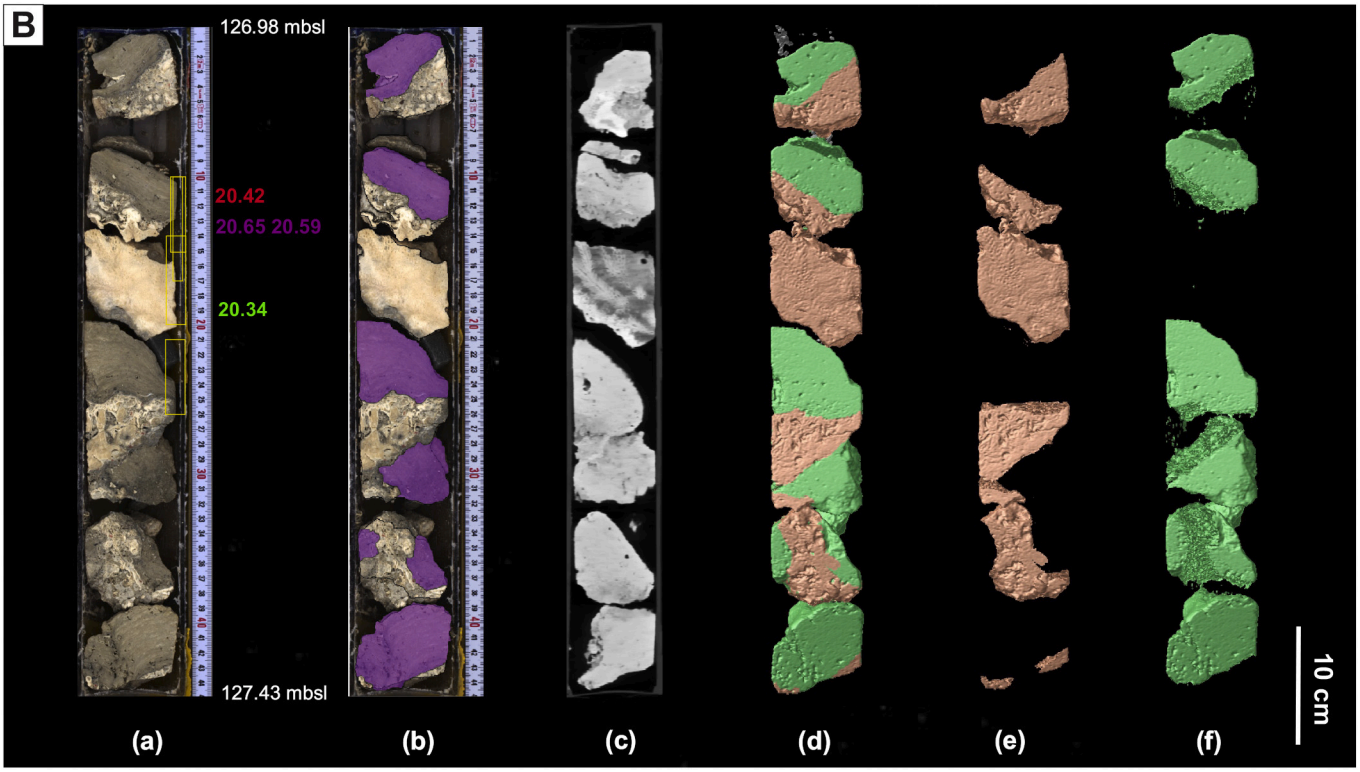

Fig. 7. Results of 3D and 2D analyses of core section M0035A-18R1A (126.98–127.43 mbsl). See caption of Fig. 6.

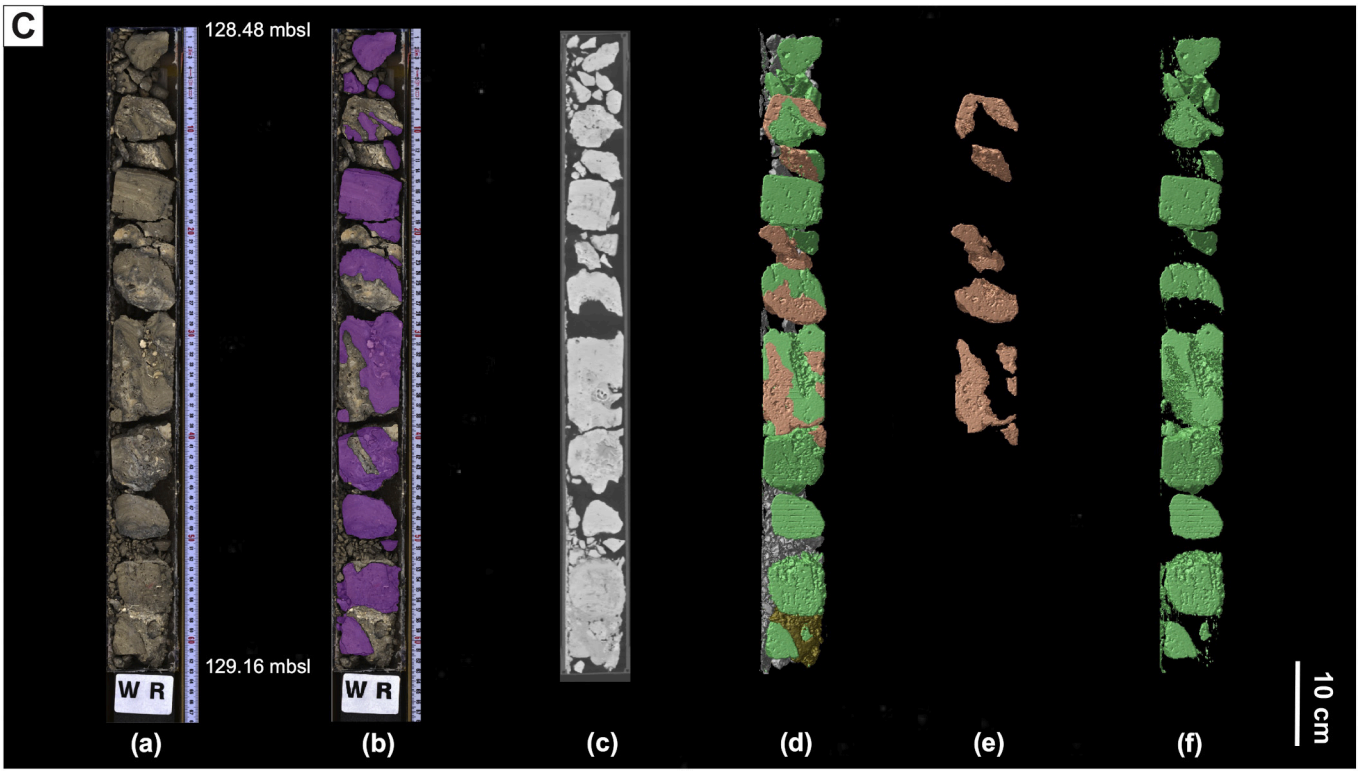

Fig. 8. Results of 3D and 2D analyses of core section M0035A-19R1A (128.48–129.16 mbsl). See caption of Fig. 6.

4.3. Comparison of the radiometric ages of microbial crusts and coralgal communities

In the majority of the analyzed cases, 14 out of 19, the uncalibrated ages of the coral/coralline algal substrates and encrusting microbialite attached to them overlap within the intervals of confidence of 95% (average uncalibrated ^{14}C age ± 2σ) (Fig. 4B, Table S1). Consequently, microbialite and its substrate are roughly coeval, i.e. microbialite developed simultaneously or immediately after (below the analytical resolution) the coral or coralline algae to which it is attached. In 4 other cases, the coralgal substrate is significantly older than the microbialite. The uncalibrated age offsets range from 168 ± 54 to 1152 ± 93 years. In only one case the uncalibrated age of the microbialite is significantly older than the underlying coralline algae (Fig. 4B, Table S1).

The topological position of the components also varies throughout the LGM and last deglacial reef sequences (Fig. 4A). For microbialites older than the associated coralgal components, the microbial crusts are mostly adjacent to, or above, the corals or coralline algae (Fig. 4B). For microbialites younger than the coralgal components, the majority of the microbial crusts overlie the coralgal components or are adjacent to them; only one instance of older microbialites under the coralgal components was recorded.

4.4. Temporal variation in microbialite crust thickness and relative abundance

4.4.1. Thickness variation through time

Thickness and abundance of microbial crusts varied throughout the cores, according to reef environments and through time between 30 and 10 kyr. Maximum thicknesses were measured on microbial crusts that display laminations in both the Hydrographer's Passage and Noggin Pass sites (Fig. 12E). The thickest crusts occur in 54B hole around ~22.5 ka with values of 11.5 cm. The average thickness, across all the cores, is 2.2 cm. Polynomial (quadratic) regression of maximum thickness variation through time shows an increasing trend from the oldest records to the crusts developed during the LGM peak, and then a decreasing trend to the youngest records. This quadratic fit is statistically significant (p value < 0.05) and its correlation coefficient is higher than that of the linear regression (Fig. 13A). We acknowledge that some of the thickness data could be skewed by cavity size.

4.4.2. Thickness variation between transects

The thickness of microbial crusts also shows variation between Hydrographer's Passage (HYD−01C) and Noggin Pass (NOG−01B) locations (Fig. 12C and D). Microbialite thickness shows a general decrease through time at Hydrographer's transect, although the maximum thickness peak (7 cm) is at ~15 ka (Fig. 12C). However, the correlation of crust thickness with age is not statistically significant at this transect (Fig. 13B). At Noggin the maximum thickness tends to increase up to the LGM and the thickness peak occurs at ~22.5 ka (11.5 cm). From the LGM peak maximum crust thickness generally decreases during deglaciation (Fig. 12D). Values of crust thickness show a significant quadratic fit with age (Fig. 13C). The average thickness also differs slightly: 2 cm in Hyd-01C and 2.4 cm in NOG−01B, but this difference is not statistically significant. In some core intervals, microbialite is scarce or only present as thin crusts (Fig. 12C and D).

4.4.3. Thickness variation between coral assemblages

Microbialite crusts occur in deep fore-reef coral assemblages (assemblage E and F, Webster et al., 2018; Humblet et al., 2019) before ~20 ka, with the thickest crusts (11.5 cm) at ~22.5 ka in coral assemblage E (Fig. 12E). After ~20 ka, microbialite crusts are mostly associated with shallow water coral assemblages (assemblage A, B and C, Webster et al., 2018; Humblet et al., 2019) and decline in thickness.

4.4.4. Relative abundance of microbial crust within associated coral assemblages through reef sequences and between transects

Regarding the distribution of microbial crusts in the reef growth sequences distinguished by Webster et al. (2018), in Reef 2, assemblage

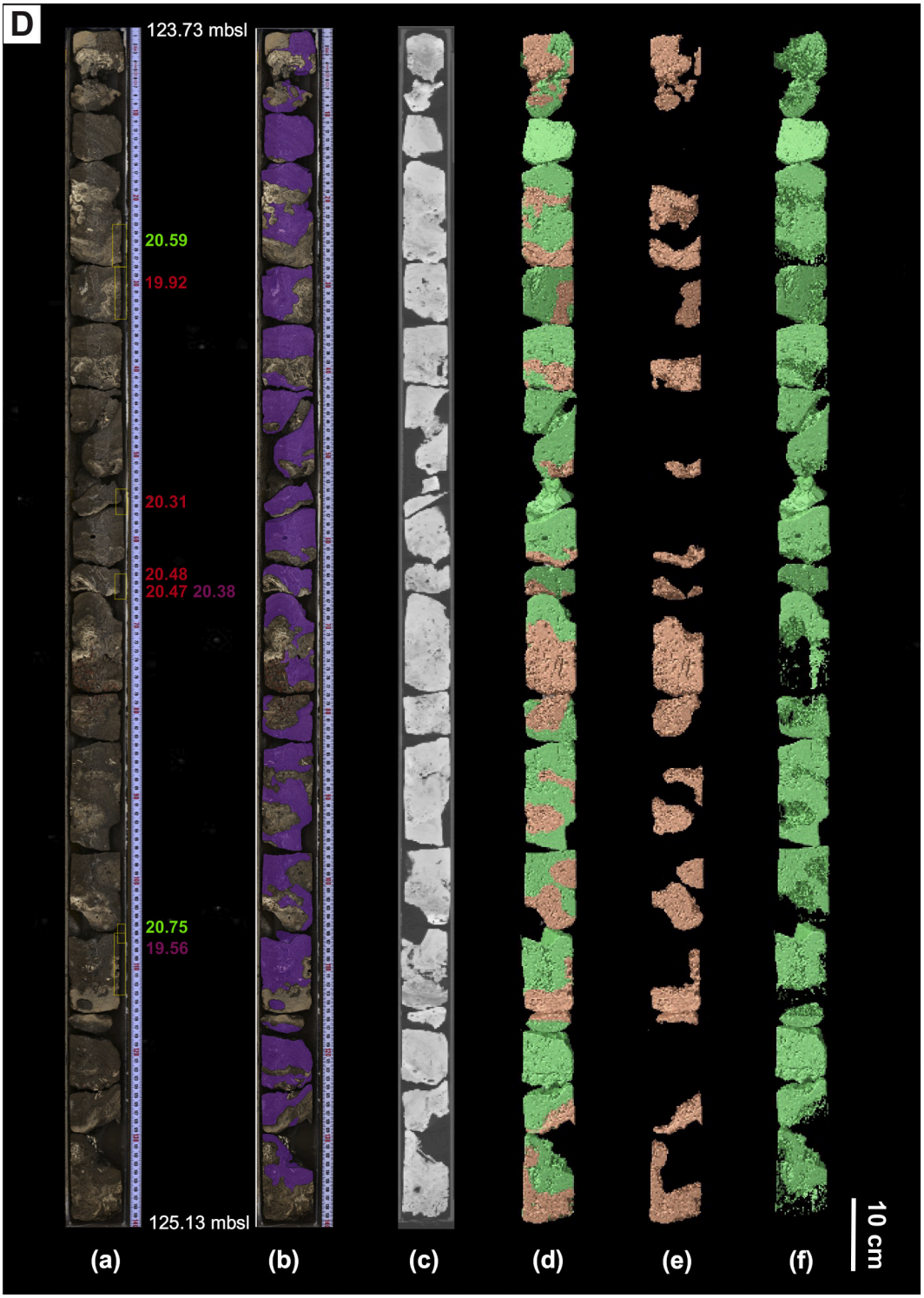

Fig. 9. Results of 3D and 2D analyses of core section M0054B-6R1A (123.73–125.13 mbsl). See caption of Fig. 6.

F has the highest content of microbial crust (67%) in HYD−01C, while in NOG−01B, the highest content (71%) occurs in assemblage E (Supplementary Fig. 2, Table 2). Crusts are more abundant in assemblage C (55%) in HYD−01C, and in assemblage B (58%) in NOG-01B in Reef 3a. In Reef 3b, the highest values are recorded in assemblage A in HYD-01C (64%) and in assemblage B in NOG-01B (40%). In Reef 4, assemblage D contains the highest relative abundance of microbial crusts in both HYD-01C (82%) and in NOG-01B (40%).

4.5. Global microbialite thickness data for the past 30 kyr

The global dataset shows that from 30 ka to 22.5 ka microbialite thickness increases to 11.5 cm, decreases between 22.5 ka and 18 ka, then increases again to ~12.5 cm at ~13.5 ka before decreasing steadily to the present (Fig. 14A). A sharp fall occurs around ~8 ka, after which no microbial crust thicker than ~5 cm is reported.

Analysis of the global data set reveals some notable geographic differences. Data from Belize shows maximum crust thickness of 3.5 cm

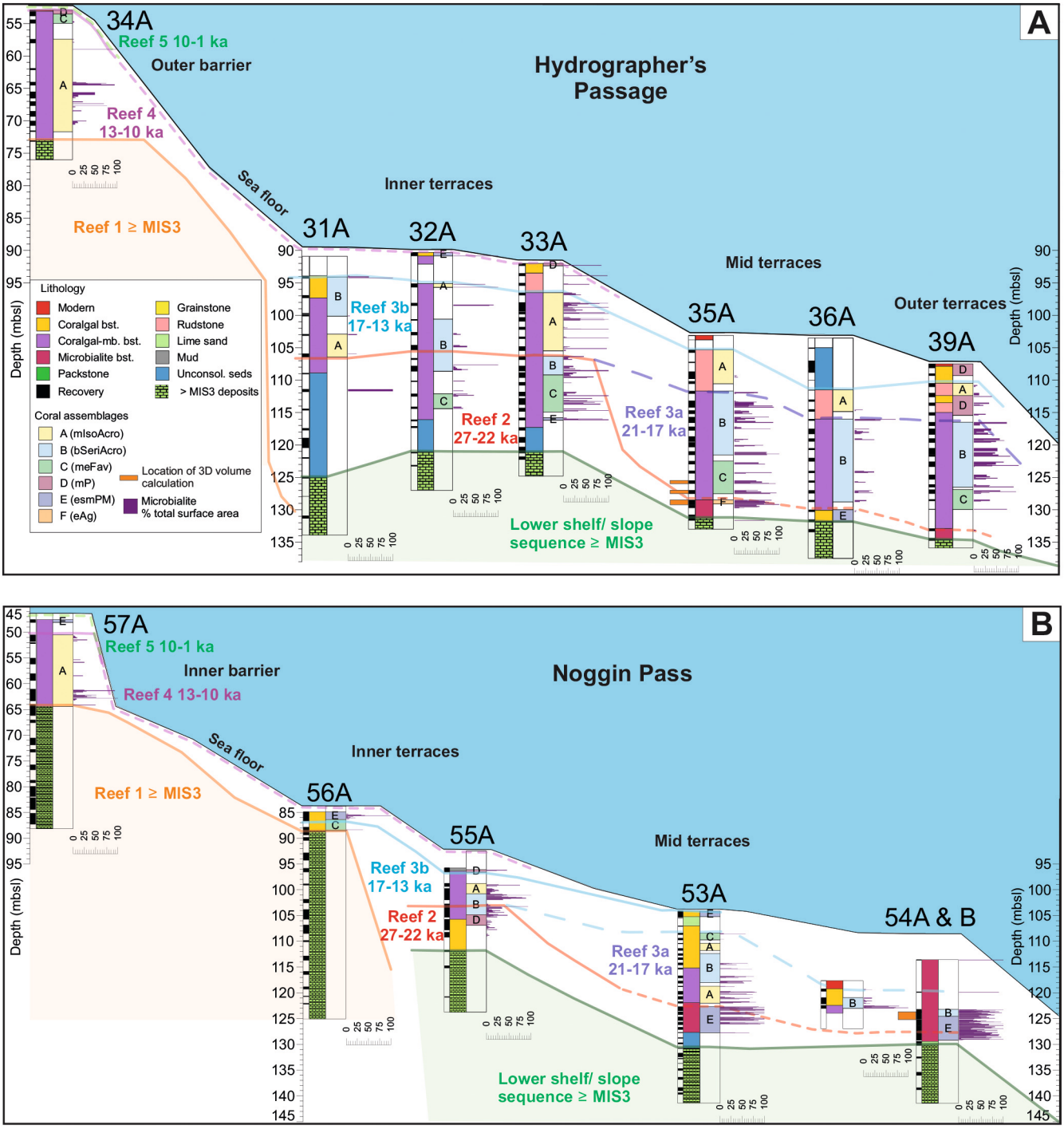

Fig. 10. Stratigraphic distribution of lithologies, coral assemblages and microbialites in (A) Hydrographer's Passage and (B) Noggin Pass transects from IODP Expedition 325 over the past 30–10 kyr. Figures were modified after Webster et al. (2018) and Braga et al. (2019). Relative surface area of microbial crust (%) is represented by purple sticks in each core. Location of 3D visually analyzed core sections is indicated by orange filled rectangles. The five main reef sequences (Reef 1–5) are represented by solid and dashed colored lines after Webster et al. (2018). (For interpretation of the references to colour in this figure legend, the reader is referred to the web version of this article.)

before a significant decrease to 1.7 cm after ~5 ka (Supplementary Fig. 1A). In the Maldives microbial crusts display a similar range of thickness with a peak of 3.5 cm at ~8 ka (Supplementary Fig. 1B). An increase followed by a decrease in microbialite thickness has also been observed in Tahiti between ~16 ka and 6 ka with a peak of 12.5 cm at ~13.5 ka (Supplementary Fig. 1 C).

Regression analysis of the global dataset, by using estimates from GBR, Tahiti, and other Holocene locations, shows a pattern similar to the one of the GBR. The best fit between maximum crust thickness and age is quadratic and indicates an increasing trend from the oldest records to the crust developed during the LGM, which have the highest average thickness, and then a generally decreasing trend to the youngest late Holocene records. The correlation is statistically significant with a p value $\ll 0.01$ (Fig. 14B).

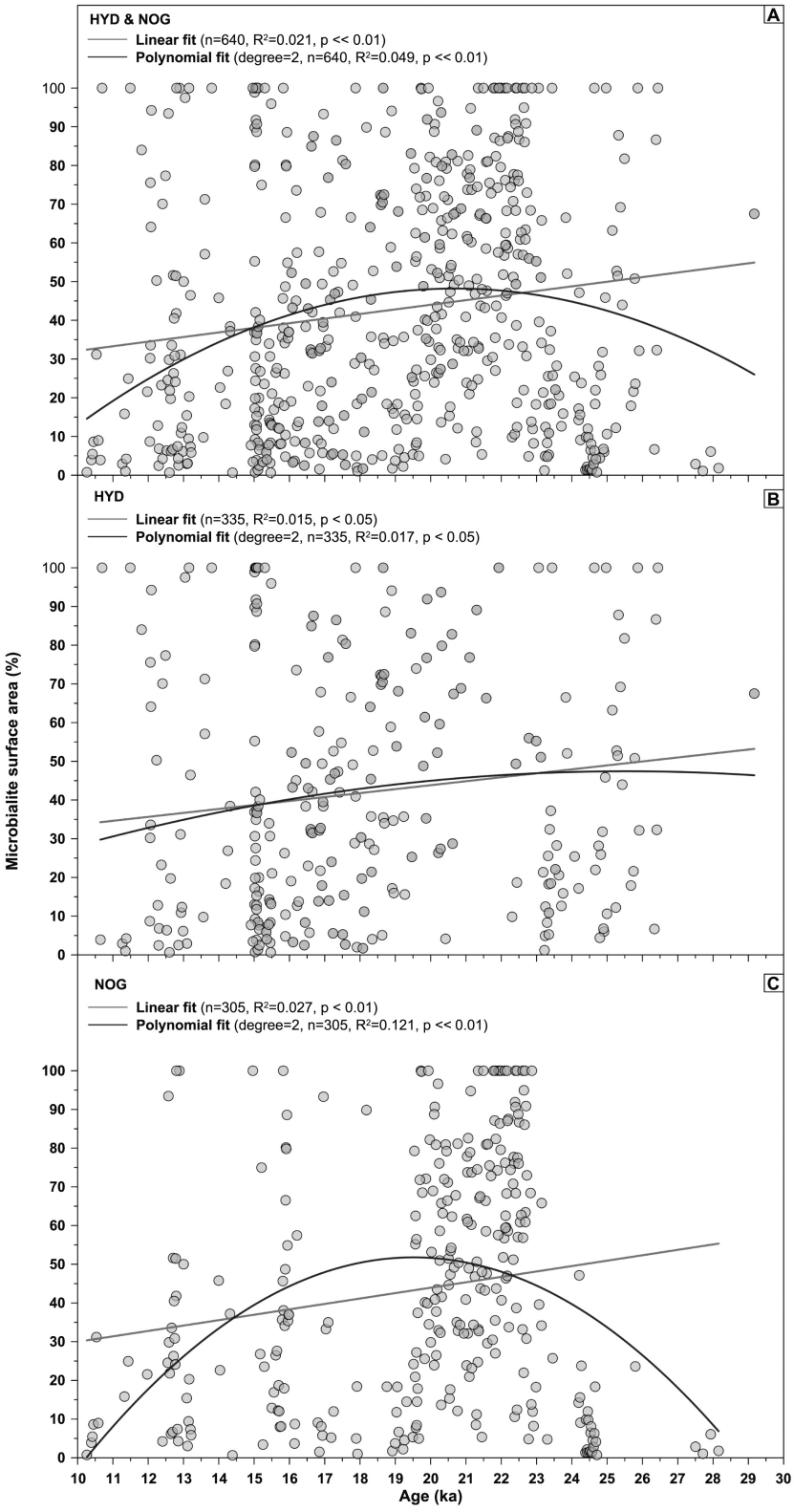

Fig. 11. Microbialite surface area in the past 30 to 10 kyr in the GBR. (A) Blue symbols represent the crust surface area data both from Hydrographer's Passage and Noggin pass locations. Regression analysis was taken on the data-set (red solid line: linear fit; blue solid line: polynomial fit). (B) Blue symbols display crust surface area just at Hydrographer's Passage. Red solid line shows the linear fit, while blue solid line represent the polynomial fit. (C) Blue symbols show crust surface area just at Noggin Pass. Red solid line represents the linear fit, while blue solid line display the polynomial fit. (For interpretation of the references to colour in this figure legend, the reader is referred to the web version of this article.)

5. Discussion

5.1. Stratigraphic distribution and abundance of microbial crusts

In both Hydrographer's Passage and Noggin Pass, Reef 3a and Reef 3b (Webster et al., 2018) display relatively high microbialite content in shallow water assemblages (assemblage A, B, and C). Presumably, this is due to their relatively more open coral frameworks containing more branching corals or corals that formed unattached plates, particularly assemblage A and B composed of branching acroporids and pocilloporids, respectively. (Table 2, Supplementary Fig. 2) (Webster et al., 2018; Humblet et al., 2019). In Reef 2 and Reef 4, deep fore-reef assemblages (assemblage E, F, and D) are associated with relatively high microbialite contents, although smaller sample size due to low recovery

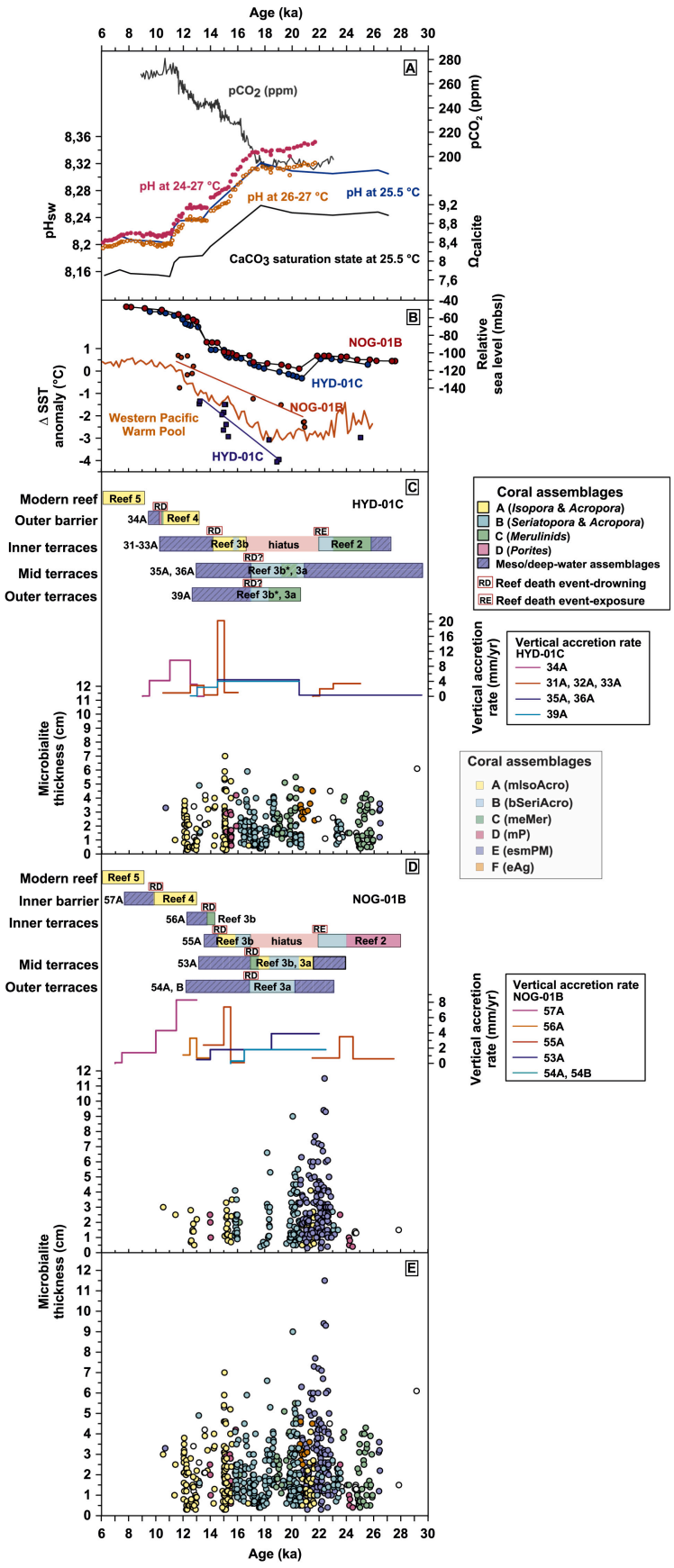

Fig. 12. Spatio-temporal distribution of microbial crusts in IODP Exp. 325 cores and possible environmental factors affecting crust development over the past 30 to 10 kyr. (A) Estimated pH and carbonate saturation state; global pH values calculated for a SST of 25.5°C (solid blue line); pH values at 24–27°C (solid pink circles) and at 26–27°C calculated for Tahiti; global calcite saturation state values calculated for a SST of 25.5°C (data adapted from Riding et al., 2014). Estimated *p*CO2 level from the high accumulation West Antarctic ice sheet core (after Marcott et al., 2014). (B) Relative sea level (RSL) curve reconstructed from IODP Exp. 325 cores (HYD−01C, red circles; NOG−01B, blue circles; after Yokoyama et al., 2018) and SST anomalies calculated for the Western Pacific Warm Pool (orange curve; Linsley et al., 2010) and for the NOG-01B and HYD-01C transects (red circles and blue squares, respectively; Felis et al., 2014). (C) Coral assemblages and rates of vertical reef accretion for HYD-01C after Webster et al. (2018) plotted against microbial crust thickness estimates in different coral assemblages from this study. (D) Coral assemblages and rates of vertical reef accretion for NOG-01B after Webster et al. (2018) plotted against the microbial crust thickness estimates in different coral assemblages from this study. (E) IODP Exp. 325 microbial crust thickness estimates for the HYD-01C and NOG-01B in the coral assemblages (described in Webster et al. (2018) and Humblet et al. (2019)). (For interpretation of the references to colour in this figure legend, the reader is referred to the web version of this article.)

may have biased our relative abundance estimate. However, this is not the case in holes 53A and 54B in Reef 2 and Reef 3a, which show a relatively high core recovery, and where the higher internal porosity of assemblage E and bioclastic breccia lithofacies, and other external controlling factors (e.g., sea-level, sea-surface temperature, nutrient supply, water chemistry, see below) led to relatively high content of microbial crust.

Therefore, our data suggest that more open frameworks with large internal open spaces led to the preferential development of microbial crusts (as inferred by Riding et al., 2014), and they can also preferentially develop in deeper environmental settings.

5.2. Timing of microbial crust formation

The radiocarbon ages from different reef components (corals, coralline algae, and microbial crusts) allow us to reconstruct the timing of microbial crust formation and assess its role in reef framework development. We find evidence for both coeval and later stage development of microbial crust within the IODP Exp. 325 reef cores (Fig. 4, Table S1).

Coeval development of coralgal communities and microbial crusts is supported by similar radiocarbon ages between coral and microbial crusts, coralline algae and microbial crusts, and their topological relationships (Fig. 4, Table S1). Microbial crusts generally overlie, or are adjacent to, associated coralgal components. Coeval ages of microbial crusts and corals or coralline algae were recorded in coralgal-microbialite boundstone (holes 33A, 35A, 39A, 55A) and microbialite boundstone (54B) characterized by different environmental and depositional settings (Braga et al., 2019).

According to Braga et al. (2019) the microbialite boundstones formed directly on the sea floor and within small cavities produced by encrusting corals and larger bioclasts in the top few centimeters of sediment in fore-reef settings, but still in the photic zone. They suggest that crust formation occurred coevally with the growth of encrusting corals and coralline algae and the accumulation of bioclasts. Microbialite boundstone in hole 54B, formed in a fore-reef setting within the photic zone and likely also reflects the repeated superposed growth of encrusting corals and microbial crusts described by Braga et al. (2019).

Braga et al. (2019) also recognised that microbial crusts in coralgal-microbialite boundstone formed in shallow water (0–20 m) where crusts veneer reef framework and fill cavities. At Tahiti (Exp. 310), Heindel et al. (2009) and Westphal et al. (2010) also reported almost identical ages of coralgal and microbialite components that suggest that coralline algae and microbial crusts filled the framework cavities immediately after coral death while still positioned in the euphotic zone. Our results suggest that microbial crusts in shallow water reef framework were most likely to develop coevally with coralgal communities within the reef framework (Hole 33A, 35A, 39A, 55A).

The later development of microbial crusts was identified exclusively in three cases in coralgal-microbialite boundstones (Hole 33A, 39A, 42A), overlying or adjacent to coralline algae and coral components, and in one case in microbialite boundstone (Hole 54B) underlying a coral (Fig. 4). Age offsets between the growth of the coralgal community and the development of these microbial crusts show 481 ± 74 yr, 541 ± 68 yr, and 1152 ± 93 delays in crust formation. The former two cases are in agreement with the results of Seard et al. (2011), who found that Tahitian shallow water microbial crusts (Exp. 310), defined as 'reefal microbialites', formed in the primary cavities of reef frameworks ~100–500 yr after the demise of the coralgal communities. Webb and Jell (1997, 2006) and Braga et al. (2019) suggested that microbial crusts in shallow-water represent the last stage of filling of the framework space in the last deglacial reef sequence. The microbialite 1152 ± 93 yr younger than the coralgal substrate could represent an extreme case of delay in cavity filling. The crust in the fore-reef boundstone (Hole 54B) much younger than the overlying coral suggests that later filling of cavities by microbialite also took place in deeper-water deposits.

Only in one case the uncalibrated age ofthe microbial crust older than that of the underlyingcoralline algae, with an offset of −384 ± 74 yr. This might be due to alteration of the coralline sample or alternatively by the incorporation of older sedimentary particles within the microbialite.

5.3. Microbial crust development in response to environmental changes

Microbial crusts have been thought to be less sensitive to changes in light and depth compared with other reef framework builders (Camoin and Montaggioni, 1994). However, recent studies have shown that their stratigraphic distribution, thickness, and morphology within reef frameworks can vary significantly in response to environmental changes (Heindel et al., 2009; Heindel et al., 2010; Seard et al., 2011, Riding et al. 2014). The IODP Exp. 325 record provides a unique opportunity to reconstruct the sensitivity of microbial crusts to major environmental changes between 10 and 30 kyr.

5.3.1. The role of sea level change and rising sea-surface temperature

Significant variations in sea-level and sea-surface temperature have been reported from the GBR over the past 30 kyr (Linsley et al., 2010; Felis et al., 2014; Yokoyama et al., 2018). Both of these environmental factors present a relatively stable condition until ~22–20.5 ka when sea-level dropped to the full extent of the LGM (Yokoyama et al., 2018). Sea-surface temperature started to continuously rise again from ~19 ka, while relative sea-level started to increase earlier, around ~20.5 ka (Fig. 12B). Felis et al. (2014) reported a 2–3 °C local temperature differences between Noggin and Hydrographer's sites, although both sites show an increasing temperature trend towards the present.

In Tahiti Camoin et al. (1999) suggested that more intense circulation and upwelling of nutrient-rich seawater, during deglacial sea-level rise stimulated microbial crust development, thereby explaining the absence of microbial crusts after 6 ka when sea-level was stable. Rising sea-level may allow faster reef accretion which, can lead to framework with more open space, but it does not necessarily lead to thicker microbialite crusts. In general, in the GBR, the highest crust thickness coincided with sea-level lowstand and low sea-surface temperature, whereas crust thickness decreased in the deglacial period. However, a local positive correlation occurs at Hydrographer's site where increasing crust thickness appears to match increase in rising sea-level and sea-surface temperature.

Microbial crusts, mainly associated with deep fore-reef coral assemblages occur around ~26 – ~20.5 ka, in Reef 2 and Reef 3a (Fig. 12C, D and E). During the development of Reef 2 (~27–22 ka), the reef formed a narrow fringing reef system characterized by slow vertical accretion (Webster et al., 2018). Records from other localities are sparse but globally this was a period of slow growth perhaps due to unfavourable environmental conditions (e.g., low accommodation space, higher sedimentation rate) (Webster et al., 2018). We suggest that slower reef accretion in these shallow reef environments led to less space for thick microbial crust development within the shallow reef framework, in contrast to deeper reef slope environments. Following the initiation of Reef 3a, conditions presumably continued to be suitable for significant microbial crust formation in deeper settings. However, with the onset of rapid deglacial sea level rise, and the rapid creation of accommodation space, faster vertical reef accretion enabled significant microbial crust formation in cavities in shallow reef environments. Microbial crusts associated with shallow water coral assemblages dominated the period from ~20.5 to 10 ka, characterized by more rapid vertical accretion during the development of Reef 3b and Reef 4 (Webster et al., 2018). We infer that microbialite formation in deeper water continued, but that conditions were better suited to crust formation in shallow-water reef cavities.

Therefore, thickness and abundance of microbial crust indicate that

the availability of accommodation space and cavities influenced crust thickness. However, while faster reef accretion creates framework with more open space, cavities, and perhaps abundant microbialite occurrence, it does not necessarily lead to thicker microbialite crusts. Indeed, there is no statistically significant correlation between crust thickness and vertical reef accretion rates at that time (Table S5). Similar results were obtained from microbialites in the Holocene reef successions of Bora Bora, French Polynesia (Gischler et al., 2020).

5.3.2. Higher nutrient and sediment supply

Increased sedimentation and nutrient supply have previously been proposed as controlling factors on the amount of microbial crusts in reef systems (Montaggioni and Camoin, 1993; Reitner, 1993; Cabioch et al., 1999; Camoin et al., 1999; Camoin et al., 2006; Heindel et al., 2009; Heindel et al., 2010; Seard et al., 2011).

Several distinct pulses of terrigenous sediment flux across the GBR margin over the past 30 kyr have been reported (Webster et al., 2018). Braga et al. (2019) observed relatively high-content of siliciclastic sediment particles, as well as high-content of land-plant biomarkers in microbial crusts. They reported higher amount of siliciclastics in Noggin Pass region (average of 9.8%) than in Hydrographer's Passage (average of 4.5%).

Exp. 325 thickness measurements display the highest value in Noggin Pass region, 11.5 cm. Nonetheless, there is no significant difference between average crust thicknesses in either transect.

Terrestrial sediment input and nutrient supply between ~23 and ~22 ka might have influenced microbial crust thickness. However, larger drainage systems are not reported in the northern central GBR at this time and the exposed land surface area during the lowest sea level was only slightly larger than in the deglacial period prior to reflooding (Braga et al., 2019). Previously published records of sediment flux to the deep sea (Dunbar et al., 2000; Dunbar and Dickens, 2003; Hinestrosa et al., 2016; Hinestrosa et al., 2019) do not show any correlation with microbialite thickness trends. For example, mass accumulation rates of fine-grained siliciclastic sediments started to increase ~14 ka and ~10 ka, while carbonate accumulation increased ~12 ka (see Hinestrosa et al., 2019 for a recent summary). However, lack of correlation with regional deep-sea sediments does not negate the possible impact of significant local sedimentation at the study sites. Nonetheless, we find no correlation with our Exp. 325 microbialite thickness data in record of Exp. 325 downhole gamma ray data presented by Hinestrosa et al. (2019). Therefore, we find no apparent correlation between sediment flux and microbial development in our study area.

5.3.3. Changes in pCO_2 level, pH and calcium carbonate saturation level

Overall, our estimates of Exp. 325 microbial crust thickness appear to show an increasing and then decreasing trend, broadly consistent with the general trends in calcium carbonate saturation state (Ω), pH, and the amount of dissolved carbon-dioxide in seawater over the last 30 kyr (Figs. 12 and 15).

According to previous studies, over geological time-scales, microbial crust development is sensitive to changes in seawater chemistry (Grotzinger, 1990; Riding and Liang, 2005). Riding et al. (2014) suggested that changes in microbial crust thicknesses during the last ~17 kyr at Tahiti and global sites could be due to natural ocean acidification. Essentially, this is a result of increased pCO_2 in seawater, low pH and carbonate saturation state with respect to carbonate minerals (Raven et al., 2005). During pCO_2 increase, Riding et al. (2014) observed a marked decline in crust thicknesses from ~14 ka, with steepest decline from 12.5 to 11 ka ago, as $\Omega_{calcite}$ fell from 8.3 to 7.8 and pH decreased by 0.04 units. These data suggest that 7.9 $\Omega_{calcite}$ represents a key threshold above which thicker crust formed and strengthened the reef frameworks. After ~9 ka, and below this threshold, no crust thicker than ~5 cm was observed in reef frameworks. Riding et al. (2014) suggested that, based on the correlation between water chemistry and microbial crusts thickness, variation in crust thickness could be used as a proxy for ocean acidification.

Our microbialite thickness measurements from the GBR over the last 30 kyr also display trends consistent with the changes in pH and $\Omega_{calcite}$ calculated for Tahiti and global conditions (Figs. 4 and 6 in Riding et al., 2014), and with the high resolution pCO_2 record from a West Antarctic ice core (Marcott et al., 2014) (Fig. 12). Indeed, there is a highly significant correlation between maximum thickness and saturation states at the same geological times (see Fig. 15). In our samples, the thickest microbial crusts occur ~22.5 ka at pH ~8.3, $\Omega_{calcite}$ ~ 9, and 195 ppm pCO_2. The GBR record shows that thick microbialites formed at pH and $\Omega_{calcite}$ of 8.23–8.32 and 8.10–9.18, respectively (Fig. 12). The general trends in crust thickness indicate an increase from the oldest records to highest values during the LGM (Fig. 13A, B and C; Fig. 14). Then, the Exp. 325 dataset shows a decline in crust thickness after ~20 ka. Thicker microbialite crusts occur within more open reef framework structure between ~12.5 and ~14.6 ka at Tahiti, while in the GBR the thickest crusts formed in massive fore-reef coral reef frameworks between ~20 and ~23 ka (Fig. 12E). A similar pattern is recorded in the global data set. Our analysis shows an overall increasing trend in crust thickness with average maxima during the LGM, and then a general decrease with different absolute values at different locations (Fig. 13D and E).

Our global data set also supports the original interpretation of Riding et al. (2014), that microbial crust thickness declined as pH and $\Omega_{calcite}$ dropped below the threshold level (7.9 for $\Omega_{calcite}$ and 8.22 for pH) (Fig. 14). Our meta-analysis also confirms that microbial crust thickness has been < 5 cm since ~9 ka. One exception, however, is observed off the Marquesas Islands. At this location, microbial crusts were reported from a deep fore-reef slope environment, and local conditions (i.e., rapid sea-level rise; Camoin et al., 2006) probably played an important role in their formation.

In the present-day context of rapid global climate change, modern microbial biofilms and mats are particularly exposed to changes in pCO_2, pH and temperature. Recent studies indicate sensitive but adaptive microbial communities that react differently to short-term environmental changes (Liu et al., 2010; Witt et al., 2011; Beltrán et al., 2016). Witt et al. (2011) suggest that changes in water chemistry could lead to shifts in bacterial biofilm species abundance and/or function. Relative abundance of some bacterial groups increases while that of others decreases in response to increased pCO_2 concentration, indicating pH sensitivity of specific bacterial groups (Witt et al., 2011).

Ries (2010) proposed that variation in seawater Mg/Ca has an effect on marine biological calcification. Laboratory experiments have shown that modern organisms that secrete aragonite and high-Mg calcite may be less negatively impacted by ocean acidification as they can maintain their calcification better via higher control over the pH and CO_3^{2-} concentration of their calcifying fluid. However, these organisms may be more vulnerable to dissolution in today's CO_2-enriched aragonite seas (Ries, 2010). Changes in microbial community composition and activity due to variation in pH and temperature (Witt et al., 2011; Beltrán et al., 2016) are likely to lead to reduced microbial crust formation, thereby weakening reef frameworks in the future.

6. Conclusions

Investigation of IODP Exp. 325 fossil coral reef cores from the GBR and a meta-analysis of global reef records, allow us to reconstruct the spatio-temporal distribution of microbial crusts in reef frameworks over the past 30 kyr. Based on 2D surface area and 3D volumetric analyses of the microbialites in the Exp. 325 reef cores, within the context of a robust new chronostratigraphic framework, we explored the timing of microbial crust formation, and its response to different environmental changes. On this basis we draw the following conclusions:

1) Analysis of CT data on a few core sections allowed us to assess the

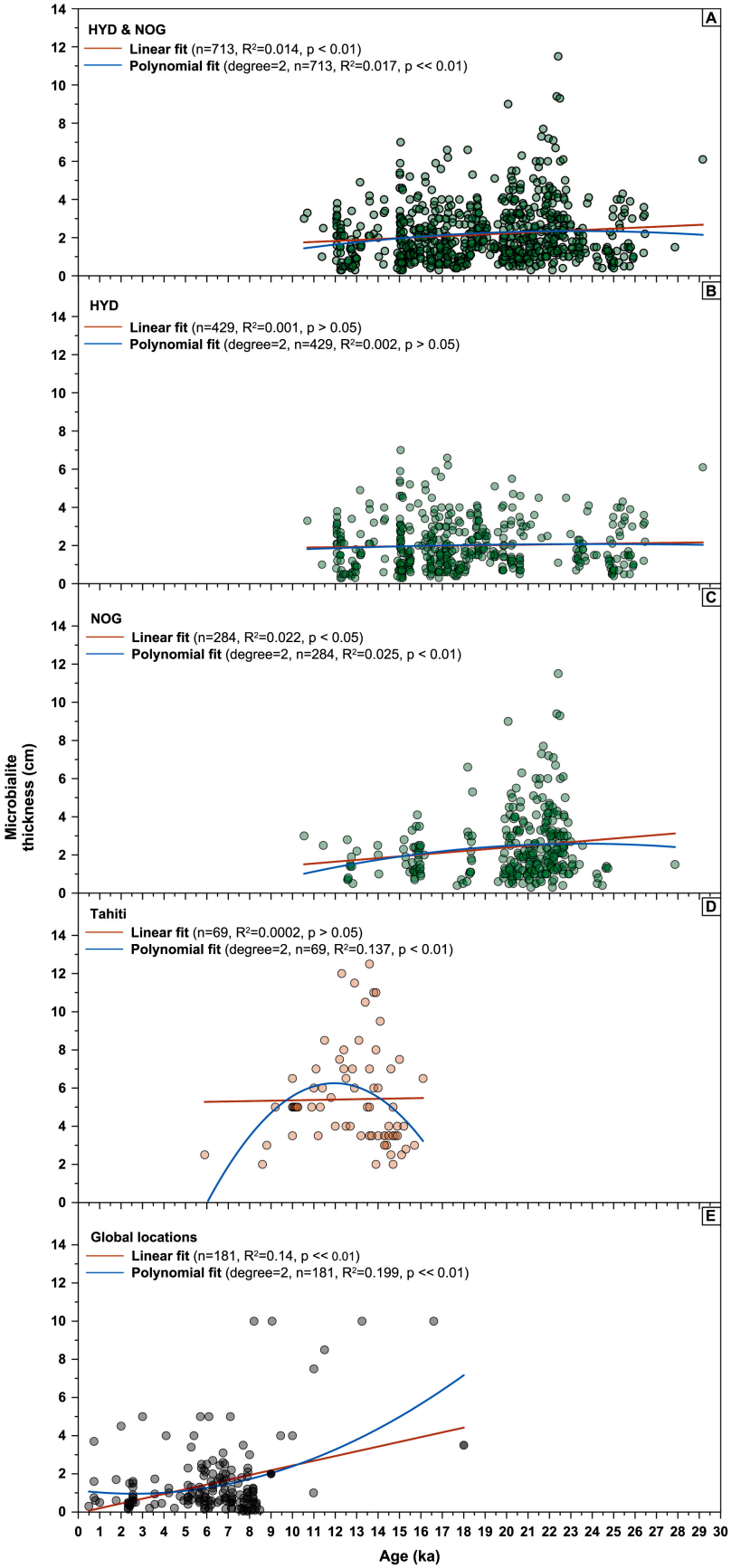

Fig. 13. Microbialite thickness over the past 30 kyr from the (A) GBR, separately from (B) Hydrographer's Passage and (C) Noggin Pass, (D) Tahiti and other (E) global locations. Red solid line represents the linear fit, while blue solid line display the polynomial fit. (For interpretation of the references to colour in this figure legend, the reader is referred to the web version of this article.)

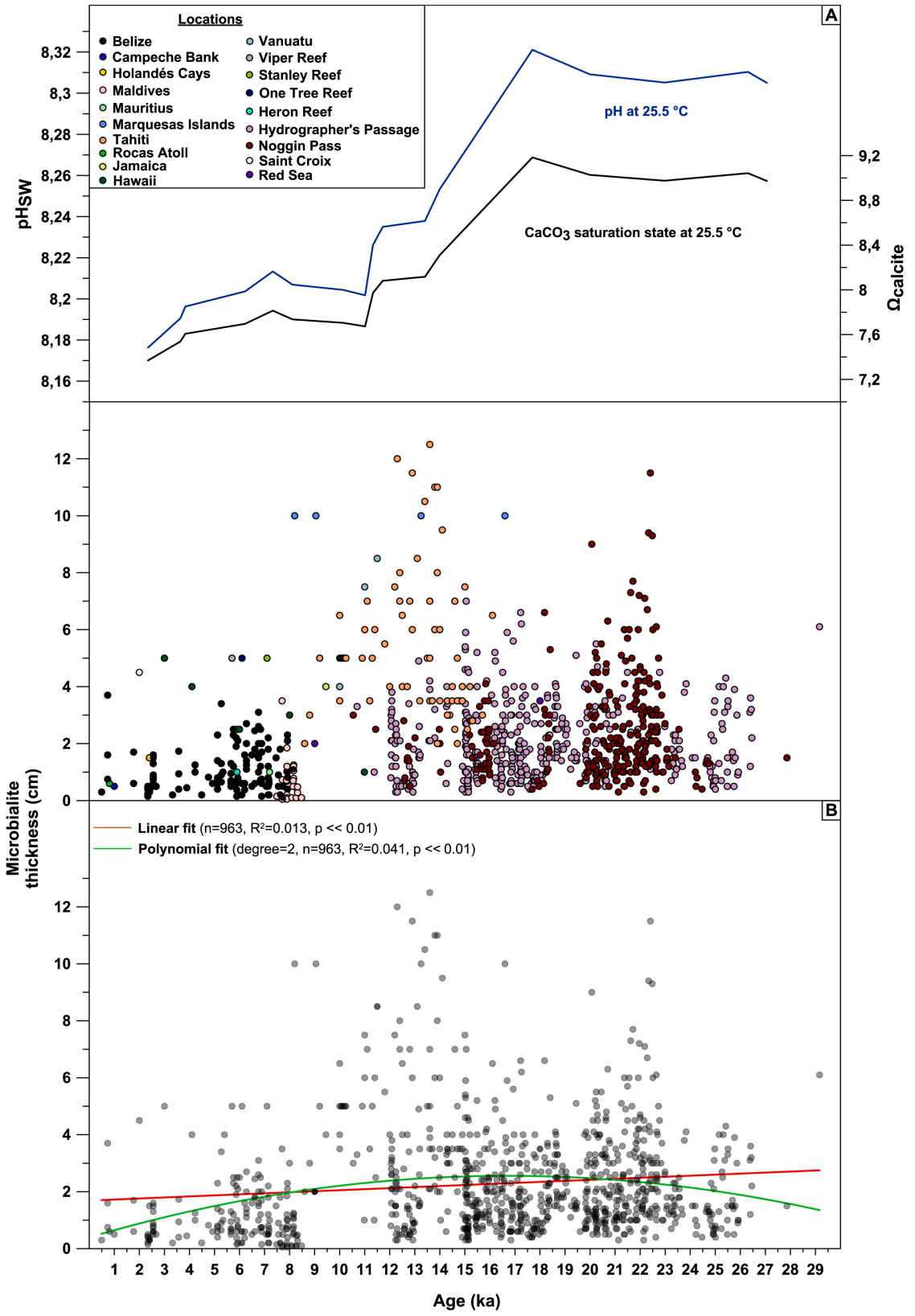

Fig. 14. Relationship between carbonate saturation state, pH and microbial crust development in reef systems over the past 30 kyr. (A) Global pH (blue solid line) and calcite saturation state (black solid line) values calculated for a SST of 25.5°C (from Riding et al., 2014) plotted against available microbial crust thickness estimates from 19 locations around the world. (B) Black symbols represent microbialite thickness values over the past 30 kyr in the GBR, Tahiti and other global locations. Red solid line shows the linear fit, while blue solid line displays the polynomial fit. (For interpretation of the references to colour in this figure legend, the reader is referred to the web version of this article.)

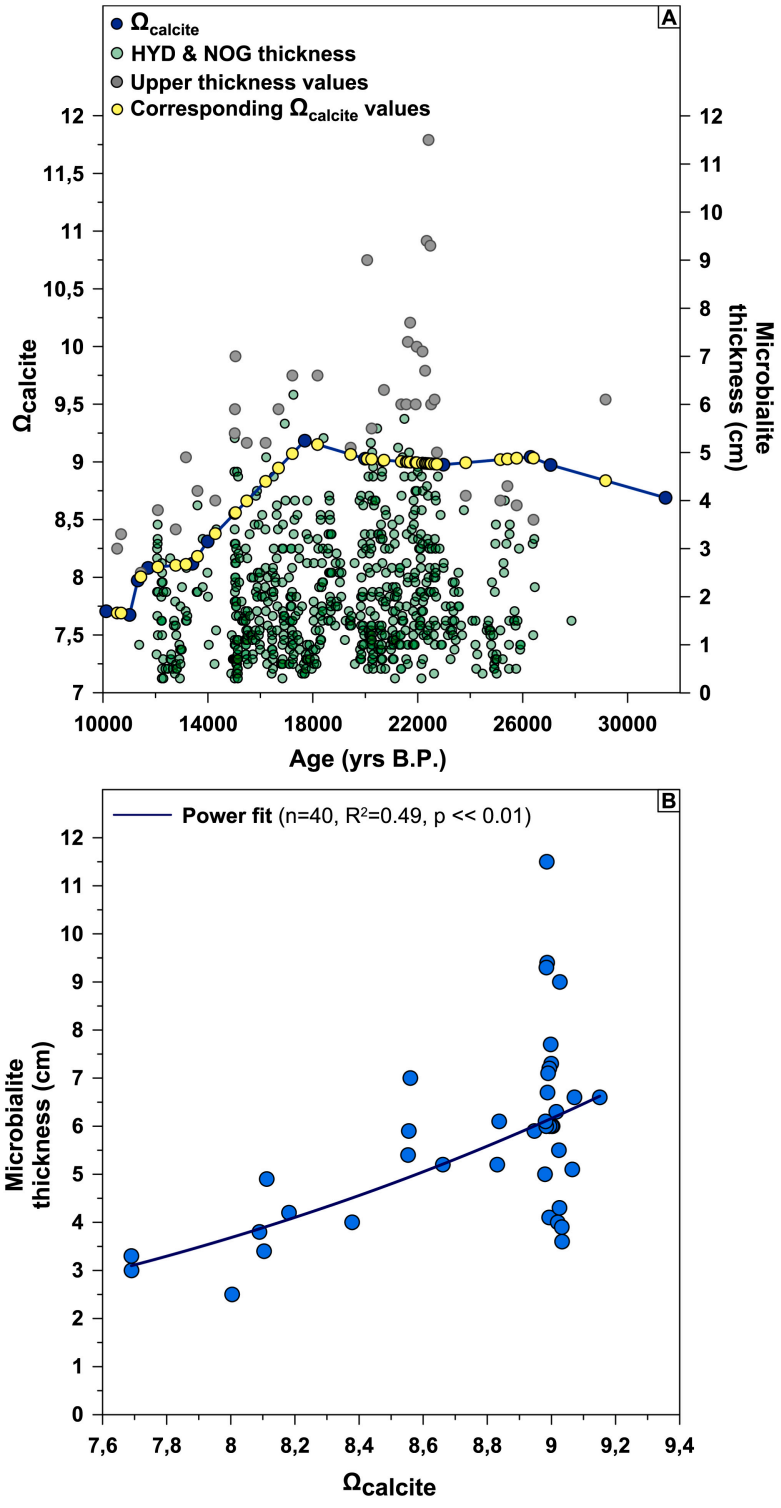

Fig. 15. Relationship between calcite saturation state and microbial crust thickness in the GBR. (A) Methodology of comparison calcite saturation state and microbialite thickness. Calculated surface ocean fluctuations in calcite saturation state during the past 30,000 years (blue symbols). Calculation based on CO_2 values from the Vostok ice core (Petit et al., 1999), assuming average seawater surface salinity of 36.7 0/00, average sea-surface temperature of 25.5°C, and average alkalinity of 2518 (μmol kg-1 seawater) throughout (from Riding et al., 2014, Fig. 6). Green symbols represent all microbialite thickness from the GBR, while grey symbols display just their upper boundary values. Linear extrapolation was used to find the corresponding calcite saturation state values to the upper boundary thickness values (yellow symbols). (B) Maximum thickness with respect to saturation states at the same geological time (using result from the previously described method). Regression analysis, power fit, was also taken on the data (blue solid line). (For interpretation of the references to colour in this figure legend, the reader is referred to the web version of this article.)

3D heterogeneity (occurrence, geometry, and volume) of the microbial crusts in the reef framework. Comparing these results to the 2D surface area estimates measured on all core sections showed that these techniques generated similar percentages of microbial crusts (average: 9.45 ± 4.5%). Therefore, the 2D surface area measurements represent a robust and efficient approach to estimate the volume of microbial crusts making up reef frameworks in the IODP Exp. 325 cores.

2) Microbial crusts in the Exp. 325 GBR record developed preferentially in deep water coral frameworks with large internal open spaces. However, they also occur in shallow environmental settings.
3) Radiometric dating of the different reef framework components (coral, coralline algae, and microbial crusts) suggest both coeval and later development (i.e., post coralgal framework development) of microbial crusts. Coeval ages indicate that microbial crusts and coralgal assemblages were able to form at the same time in both shallow water and deep, fore-reef settings. In three cases, markedly later crust development was identified in shallow water, 481 ± 74 yr to 1152 ± 93 after the underlying/ adjacent coralgal community demise.

Table 2
Summary of microbial crust surface area (%) in each coral assemblages by reef sequences.

Reef sequences	Location/ transect	Core ID	Coral assemblages	Depth (mbsl)	Microbialite surface area (%)
Reef 2	HYD-01C	M0032A	B	105.5–108.64	8.45
			C	112.1–114.41	22.31
		M0033A	B	106.3–109.2	18.22
			C	109.2–114.9	38.74
			E	115.8–116.19	26.46
		M0035A	F	128.48–129.11	67.02
		M0036A	E	130–131.87	3.06
Reef 3a	HYD-01C	M0035A	B	111.68–121.54	37.81
			C	122.48–127.53	55.19
		M0036A	B	116–128.78	26.23
		M0039A	B	116.48–126.52	39.64
			C	126.88–129.96	42.13
Reef 3b	HYD-01C	M0031A	B	94.08–100.14	35.68
			A	102.9–106.45	19.32
		M0032A	A	95.1–95.7	64.04
			B	100.6–105.5	19.06
		M0033A	A	96.5–105.48	28.53
		M0035A	A	105.3–110.56	5.95
		M0036A	A	111.5–114.85	8.86
		M0039A	A	110.48–112.38	8.67
			D	112.39–115.44	25.52
Reef 4	HYD-01C	M0034A	C	53.54–54.97	3.91
			A	57.4–71.68	22.92
		M0032A	E	90.3–90.85	50.00
		M0033A	D	92–92.37	81.60
Reef 2	NOG-01B	M0055A	B	103–104.82	24.32
			D	104.82–106.94	10.44
		M0053A	E	122.7–127.75	71.26
		M0054B	E	127.5–129.2	60.63
Reef 3a	NOG-01B	M0053A	C	108.4–109.74	13.77
			B	112.4–118.02	31.49
			A	118.7–122.03	43.35
		M0054A	B	120.95–123.03	27.66
		M0054B	B	123.23–124.55	57.96
			E	124.55–127.5	53.16
Reef 3b	NOG-01B	M0056A	C	86.36–88.52	3.41
		M0055A	A	98.75–100.8	17.94
			B	100.8–103	39.59
Reef 4	NOG-01B	M0057A	A	50.55–64.45	19.42
		M0056A	E	84.85–86.36	15.93
		M0055A	D	96.12–96.57	40.09

4) Temporal changes in microbialite crust thickness were observed in the IODP Exp. 325 dataset: crust thickness reached a maximum of 11.5 cm at ~22.5 ka before decreasing to ~3 cm in younger core sections. Combined with our global meta-analysis, this represents the most comprehensive reef record of microbialite thickness for the past 30 kyr.
5) Both GBR and global data show an overall increasing trend from the oldest records to the LGM peak, and then a generally decreasing trend during deglaciation and Holocene. The temporal trends in maximum thickness of GBR microbialites display a significant positive correlation with carbonate saturation level and pH, and inverse correlation with increasing pCO_2 level. Together with the lack of clear correlation with other environmental parameters - such as nutrient and sediment supply, rising sea-surface temperature and sea-level – our results suggest that microbial crust formation was likely influenced by ocean chemistry conditions over the past 30 kyr. As ocean $\Omega_{calcite}$ and pH dropped below key thresholds (~7.9 and ~8.22, respectively) during the past ~9 kyr, microbialite crusts in reef frameworks became relatively thin (< ~5 cm).

Supplementary data to this article can be found online at https://doi.org/10.1016/j.margeo.2020.106312.

Declaration of Competing Interest

The authors declare that they have no known competing financial interests or personal relationships that could have appeared to influence the work reported in this paper.

Acknowledgements

We would like to thank IODP for the drilling operations and members of the Bremen Core Repository for their assistance during the onshore science party. We acknowledge the facilities and the scientific and technical assistance of the Australian Microscopy & Microanalysis Research Facility at the Australian Centre for Microscopy & Microanalysis at the University of Sydney. Financial support for this research was provided by the Australian Research Council (grants DP1094001; DP120101793) and ANZIC (IODP) to J.M.W. and Tempus Közalapítvány to Zs.Sz.

References

Abbey, E., Webster, J.M., Beaman, R.J., 2011. Geomorphology of submerged reefs on the shelf edge of the Great Barrier Reef: the influence of oscillating Pleistocene sea-levels. Mar. Geol. 288 (1–4), 61–78.
Beltrán, Y., Cerqueda-García, D., Taş, N., Thomé, P.E., Iglesias-Prieto, R., Falcón, L.I., 2016. Microbial composition of biofilms associated with lithifying rubble of *Acropora palmata* branches. FEMS Microbiol. Ecol. 92 (1).
Braga, J.C., Puga-Bernabeu, A., Heindel, K., Patterson, M.A., Birgel, D., Peckmann, J., Sánchez-Almazo, I.M., Webster, J.M., Yokoyama, Y., Riding, R., 2019. Microbialites in Last glacial maximum and deglacial reefs of the Great Barrier Reef (IODP Expedition 325, NE Australia). Palaeogeogr. Palaeoclimatol. Palaeoecol. 514, 1–17.
Cabioch, G., Taylor, F., Correge, T., Rect, J., Edwards, L., Burr, G.S., Cornec, F.L., Banks, K.A., 1999. Occurence and significance of microbialites in the uplift Tasmaloum reef (SW Espiritu, Santo, SW Pacific). Sediment. Geol. 126, 305–316.
Cabioch, G., Camoin, G., Webb, G.E., Le Cornec, F., Garcia Molina, M., Pierre, C., Joachimski, M.M., 2006. Contribution of microbialites to the development of coral reefs during the last deglacial period: case study from Vanuatu (South-West Pacific). Sediment. Geol. 185 (3–4), 297–318.
Camoin, G.F., Montaggioni, L.F., 1994. High energy coralgal-stromatolite frameworks from Holocene reefs (Tahiti, French Polynesia). Sedimentology 41 (4), 655–676.
Camoin, G., Gautret, P., Monaggioni, L.F., Cabioch, G., 1999. Nature and environmental significance of microbialites in Quaternary reefs: the Taihiti paradox. Sediment. Geol. 126, 271–304.
Camoin, G., Cabioch, G., Eisenhauer, A., Braga, J.C., Hamelin, B., Lericolais, G., 2006. Environmental significance of microbialites in reef environments during the last deglaciation. Sediment. Geol. 185 (3–4), 277–295.
Carlson, W.D., 2006. Three-dimensional imaging of earth and planetary materials. Earth Planet. Sci. Lett. 249 (3–4), 133–147.
Cook, G.T., Ascough, P.L., Bonsall, C., Hamilton, W., Russell, N., Sayle, K.L., Scott, E., Bownes, J.M., 2015. Best practice methodology for 14 C calibration of marine and mixed terrestrial/marine samples. Quat. Geochronol. 27, 164–171.
Dunbar, G.B., Dickens, G.R., 2003. Massive siliciclastic discharge to slopes of the Great Barrier Reef platform during sea-level transgression: constraints from sediment cores between 15[deg]S and 16[deg]S latitude and possible explanations. Sediment. Geol. 162 (1–2), 141–158.
Dunbar, G.B., Dickens, G.R., Carter, R.M., 2000. Sediment flux across the Great Barrier Reef Shelf to the Queensland Trough over the last 300 ky. Sediment. Geol. 133 (1–2), 49.
Felis, T., McGregor, H.V., Linsley, B.K., Tudhope, A.W., Gagan, M.K., Suzuki, A., Inoue, M., Thomas, A.L., Esat, T.M., Thompson, W.G., 2014. Intensification of the meridional temperature gradient in the Great Barrier Reef following the Last glacial maximum. Nat. Commun. 5, 4102.
Ginsburg, R.N., 1983. Geological and biological roles of cavities in coral reefs. In: Barnes, D.J. (Ed.), Perspectives on Coral Reefs, pp. 148–153 Austral. Inst. Mar. Sci.
Gischler, E., Thomas, A.L., Droxler, A.W., Webster, J.M., Yokoyama, Y., Schöne, B.R., 2013. Microfacies and diagenesis of older Pleistocene (pre-last glacial maximum) reef deposits, Great Barrier Reef, Australia (IODP Expedition 325): a quantitative approach. Sedimentology 60 (6), 1432–1466.
Gischler, E., Birgel, D., Brunner, B., Peckmann, J., 2020. Microbialite occurrence and patterns in Holocene reefs of Bora Bora, Society Islands. Palaios 35 (6), 262–276.
Grotzinger, J.P., 1990. Geochemical model for Proterozoic stromatolite decline. Am. J. Sci. 290 (A), 80–103.
Heindel, K., Wisshak, M., Westphal, H., 2009. Microbioerosion in Tahitian reefs: a record of environmental change during the last deglacial sea-level rise (IODP 310). Lethaia 42 (3), 322–340.
Heindel, K., Birgel, D., Peckmann, J., Kuhnert, H., Westphal, H., 2010. Formation of Deglacial Microbialites in Coral Reefs Off Tahiti (IODP 310) involving sulfate-reducing bacteria. Palaios 25 (10), 618–635.
Heindel, K., Birgel, D., Brunner, B., Thiel, V., Westphal, H., Gischler, E., Ziegenbalg, S.B., Cabioch, G., Sjövall, P., Peckmann, J., 2012. Post-glacial microbialite formation in

coral reefs of the Pacific, Atlantic, and Indian Oceans. Chem. Geol. 304–305 (0), 117–130.
Hinestrosa, G., Webster, J.M., Beaman, R.J., 2016. Postglacial sediment deposition along a mixed carbonate-siliciclastic margin: new constraints from the drowned shelf-edge reefs of the Great Barrier Reef, Australia. Palaeogeogr. Palaeoclimatol. Palaeoecol. 446, 168–185.
Hinestrosa, G., Webster, J.M., Beaman, R.J., 2019. Spatio-temporal patterns in the postglacial flooding of the Great Barrier Reef shelf, Australia. Cont. Shelf Res. 173, 13–26.
Hughes, T.P., Rodrigues, M.J., Bellwood, D.R., Ceccarelli, D., Hoegh-Guldberg, O., McCook, L., Moltschaniwskyj, N., Pratchett, M.S., Steneck, R.S., Willis, B., 2007. Phase shifts, herbivory, and the resilience of coral reefs to climate change. Curr. Biol. 17 (4), 360–365.
Hughes, T.P., Graham, N.A., Jackson, J.B., Mumby, P.J., Steneck, R.S., 2010. Rising to the challenge of sustaining coral reef resilience. Trends Ecol. Evol. 25 (11), 633–642.
Humblet, M., Potts, D., Webster, J., Braga, J., Iryu, Y., Yokoyama, Y., Bourillot, R., Séard, C., Droxler, A., Fujita, K., 2019. Late glacial to deglacial variation of coralgal assemblages in the Great Barrier Reef, Australia. Global Planet. Change 174, 70–91.
Insalaco, E., 1998. The descriptive nomenclature and classification of growth fabrics in fossil scleractinian reef. Sediment. Geol. 118, 159–186.
Jell, J.S., Webb, G.E., 2012. Geology of heron island and adjacent reefs, Great Barrier Reef, Australia. Episodes 35 (1), 110–119.
Ketcham, R.A., Carlson, W.D., 2001. Acquisition, optimization and interpretation of X-ray computed tomographic imagery: applications to the geosciences. Comput. Geosci. 27 (4), 381–400.
Land, L.S., Goreau, T.F., 1970. Submarine lithification of Jamaican reefs. J. Sediment. Res. 40 (1).
Linsley, B.K., Rosenthal, Y., Oppo, D.W., 2010. Holocene evolution of the Indonesian throughflow and the western Pacific warm pool. Nat. Geosci. 3 (8), 578.
Liu, J., Weinbauer, M.G., Maier, C., Dai, M., Gattuso, J.-P., 2010. Effect of ocean acidification on microbial diversity and on microbe-driven biogeochemistry and ecosystem functioning. Aquat. Microb. Ecol. 61 (3), 291–305.
Macintyre, I.G., 1977. Distribution of submarine cements in a modern Caribbean fringing reef, Galeta Point, Panama. J. Sediment. Res. 47 (2), 503–516.
Marcott, S.A., Bauska, T.K., Buizert, C., Steig, E.J., Rosen, J.L., Cuffey, K.M., Fudge, T., Severinghaus, J.P., Ahn, J., Kalk, M.L., 2014. Centennial-scale changes in the global carbon cycle during the last deglaciation. Nature 514 (7524), 616.
Montaggioni, L.F., Camoin, G.F., 1993. Stromatolites associated with coralgal communities in Holocene high- energy reefs. Geology 21 (2), 149–152.
Pandolfi, J.M., Bradbury, R.H., Sala, E., Hughes, T.P., Bjorndal, K.A., Cooke, R.G., McArdle, D., McClenachan, L., Newman, M.J.H., Paredes, G., Warner, R.R., Jackson, J.B.C., 2003. Global trajectories of the long-term decline of coral reef ecosystems. Science 301 (5635), 955–958.
Petit, J.R., Jouzel, J., Raynaud, D., Barkov, N.I., Barnola, J-M., Basile, I., Bender, M., Chappellaz, J., Davis, M., Delaygue, G., Delmotte, M., Kotlyakov, V.M., Legrand, M., Lipenkov, V.Y., Lorius, C., Pepin, L., Ritz, C., Saltzman, E., Stievenard, M., 1999. Climate and atmospheric history of the past 420,000 years from the Vostok ice core, Antarctica. Nature 429–436.
Pigott, J.D., Land, L.S., 1986. Interstitial water chemistry of Jamaican reef sediment: sulfate reduction and submarine cementation. Mar. Chem. 19 (4), 355–378.
Raven, J., Caldeira, K., Elderfield, H., Hoegh-Guldberg, O., Liss, P., Riebesell, U., Shepherd, J., Turley, C., Watson, A., 2005. Ocean Acidification Due to Increasing Atmospheric Carbon Dioxide. The Royal Society.
Reimer, P.J., Bard, E., Bayliss, A., Beck, J.W., Blackwell, P.G., Ramsey, C.B., Buck, C.E., Cheng, H., Edwards, R.L., Friedrich, M., 2013. IntCal13 and Marine13 radiocarbon age calibration curves 0–50,000 years cal BP. Radiocarbon 55 (4), 1869–1887.
Reitner, J., 1993. Modern cryptic microbialite/metazoan facies from Lizard Island (Great Barrier Reef, Australia) formation and concepts. Facies 29 (1), 3–39.
Riding, R., 1991. Classification of Microbial Carbonates: Calcareous Algae and Stromatolites. vol. 2. pp. 1–51.
Riding, R., Liang, L., 2005. Geobiology of microbial carbonates: metazoan and seawater saturation state influences on secular trends during the Phanerozoic. Palaeogeogr. Palaeoclimatol. Palaeoecol. 219 (1–2), 101–115.
Ries, J.B., 2010. Geological and experimental evidence for secular variation in seawater Mg/Ca (calcite-aragonite seas) and its effects on marine biological calcification. Biogeosciences 7 (9), 2795–2849.
Riding, R., 2011. Reefal microbial crusts. In: Hopley, D. (Ed.), Encyclopedia of Modern Coral Reefs: Structure, Form and Process: Heidelberg, Encyclopedia of Earth Science Series. Springer, pp. 911–915.
Petit, J.R., Liang, L., Braga, J., 2014. Millennial-scale ocean acidification and late Quaternary decline of cryptic bacterial crusts in tropical reefs. Geobiology 387–405.
Seard, C., Camoin, G., Yokoyama, Y., Matsuzaki, H., Durand, N., Bard, E., Sepulcre, S., Deschamps, P., 2011. Microbialite development patterns in the last deglacial reefs from Tahiti (French Polynesia; IODP Expedition# 310): implications on reef framework architecture. Mar. Geol. 279 (1), 63–86.
Stuiver, M., Braziunas, T.F., 1993. Modeling atmospheric 14 C influences and 14 C ages of marine samples to 10,000 BC. Radiocarbon 35 (1), 137–189.
Webb, G.E., Jell, J.S., 1997. Cryptic microbialite in subtidal reef framework and intertidal solution cavities in beachrock, Heron Reef, Great Barrier Reef, Australia: preliminary observations. Facies 36, 219–223.
Webb, G.E., Jell, J.S., 2006. Growth Rate of Holocene Reefal Microbialites? Implications for Use as Environmental Proxies, Heron Reef Southern Great Barrier Reef, Australian Earth Science Convention Extended Abstracts. vol. 2006. pp. 1–3 Melbourne.
Webb, G.E., Kamber, B.S., 2000. Rare earth elements in Holocene reefal microbialites: a new shallow seawater proxy. Geochim. Cosmochim. Acta 64 (9), 1557–1565.
Webb, G.E., Baker, J.C., Jell, J.S., 1998. Inferred syngenetic textural evolution in Holocene cryptic reefal microbialites, Heron Reef, Great Barrier Reef, Australia. Geology 26 (4), 355–358.
Webster, J.M., Braga, J.C., Clague, D.A., Gallup, C., Hein, J.R., Potts, D.C., Renema, W., Riding, R., Riker-Coleman, K., Silver, E., Wallace, L.M., 2009. Coral reef evolution on rapidly subsiding margins. Glob. Planet. Chang. 66 (1–2), 129–148.
Webster, J.M., Yokoyama, Y., Cotterill, C., Expedition 325 Scientists, 2011. Proceedings of the Integrated Ocean Drilling Program Volume 325 Expedition Reports Great Barrier Reef Environmental Changes, Proceedings of the Integrated Ocean Drilling Program, Integrated Ocean Drilling Program Management International, Inc., for the Integrated Ocean Drilling Program.
Webster, J.M., Braga, J.C., Humblet, M., Potts, D.C., Iryu, Y., Yokoyama, Y., Fujita, K., Bourillot, R., Esat, T.M., Fallon, S., Thompson, W.G., Thomas, A.L., Kan, H., McGregor, H.V., Hinestrosa, G., Obrochta, S.P., Lougheed, B.C., 2018. Response of the Great Barrier Reef to sea level and environmental changes over the past 30,000 years. Nat. Geosci. 11 (6), 426.
Westphal, H., Heindel, K., Brandano, M., Peckmann, J., 2010. Genesis of microbialites as contemporaneous framework components of deglacial coral reefs, Tahiti (IODP 310). Facies 56 (3), 337–352.
Witt, V., Wild, C., Anthony, K., Diaz-Pulido, G., Uthicke, S., 2011. Effects of ocean acidification on microbial community composition of, and oxygen fluxes through, biofilms from the Great Barrier Reef. Environ. Microbiol. 13 (11), 2976–2989.
Woodroffe, C.D., Webster, J.M., 2014. Coral reefs and sea-level change. Mar. Geol. 352, 248–267.
Yokoyama, Y., Webster, J.M., Cotterill, C., Braga, J.C., Jovane, L., Mills, H., Morgan, S., Suzuki, A., Expedition 325 Scientists, 2011. IODP Expedition 325: Great Barrier Reefs reveals past sea-level, climate and environmental changes during the end of the last Ice age. Sci. Drill. 12, 32–45.
Yokoyama, Y., Esat, T.M., Thompson, W.G., Thomas, A.L., Webster, J.M., Miyairi, Y., Sawada, C., Aze, T., Matsuzaki, H., Okuno, J.I., Fallon, S., Braga, J.-C., Humblet, M., Iryu, Y., Potts, D.C., Fujita, K., Suzuki, A., Kan, H., 2018. Rapid glaciation and a two-step sea-level plunge into the Extreme Glacial Maximum. Nature 559 (7715), 603.